Transcription-dependent domain-scale 3D genome organization in dinoflagellates

Georgi K. Marinov[1,*,#], Alexandro E. Trevino[3,7,*], Tingting Xiang[2,8,*], John R. Pringle[1], Anshul Kundaje[1,6], Arthur R. Grossman[2], and William J. Greenleaf[1,3,4,5,#]

[1] *Department of Genetics, Stanford University, Stanford, California 94305, USA*
[2] *Carnegie Institution for Science, Department of Plant Biology, Stanford, California 94305, USA*
[3] *Center for Personal Dynamic Regulomes, Stanford University, Stanford, California 94305, USA*
[4] *Department of Applied Physics, Stanford University, Stanford, California 94305, USA*
[5] *Chan Zuckerberg Biohub, San Francisco, California, USA*
[6] *Department of Computer Science, Stanford University, Stanford, California 94305, USA*
[7] *Department of Bioengineering, Stanford University, Stanford, California 94305, USA*
[8] *Department of Biological Sciences, University of North Carolina at Charlotte, Charlotte, NC 28223, USA*
[*] *These authors contributed equally to this work*
[#] *Corresponding author*

Abstract

Dinoflagellate chromosomes represent a unique evolutionary experiment, as they exist in a permanently condensed, liquid crystalline state, are not packaged by histones, and contain genes organized into polycistronic arrays, with minimal transcriptional regulation. We analyze the 3D genome of *Breviolum minutum*, and find large topological domains without chromatin loops, demarcated by convergent gene array boundaries ("dinoTADs). Transcriptional inhibition degrades dinoTADs, implicating transcription-induced supercoiling as the primary topological force in dinoflagellates.

The three-dimensional (3D) genome architecture of cells has functional consequences for gene regulation, organismal development, replication, and mutational processes. Mechanisms known to drive genome folding in eukaryotes include constraints on cohesin-mediated loop extrusion – imposed by CTCF in vertebrates – that generate topologically associating domains (TADs), and self-associations between similar chromatin states that form compartments[1]. However, the extent to which genome function itself may influence genome folding, for example through transcriptional activity, is poorly understood. There has also been little exploration of 3D organization across eukaryotes, even though major deviations from conventional norms are known to exist, presenting natural experiments that may reveal deeper underlying organizational principles masked in other lineages.

Dinoflagellates are the most radical such departure. They are a diverse, widespread clade playing major roles in aquatic ecosystems, for example, as symbiointes of corals, providing the metabolic basis for reef ecosystems. Dinoflagellates possess numerous highly divergent molecular features[2], including, uniquely among eukaryotes, the loss of nucleosomal packaging of chromatin. Histones are extremely conserved across eukaryotes, were present in their current form already in the Last Eukaryotic Common Ancestor[3], and they and their posttranslational modifications are pivotal to all biochemical processes involving chromatin.

Dinoflagellates are the sole known exception. Their chromosomes exist in a liquid crystalline state, are permanently condensed throughout the cell cycle, and, although highly divergent histone genes are retained in their genomes[4], a combination of virus-derived nucleoproteins and bacterial-derived histone-like proteins have taken over as main packaging components[5]. Dinoflagellate genomes are often huge (up to ≥100 Gbp), genes are organized into polycistronic gene arrays, individual mRNAs are generated through *trans*-splicing, and transcriptional regulation is largely absent. These fascinating features simultaneously pose intriguing questions regarding the adaptation of transcriptional and regulatory mechanisms to the absence of nucleosomes, and provide a unique opportunity to explore the biophysical forces underlying genomic organization in the context of a large eukaryotic genome nearly devoid of nucleosomes.

To explore these questions, we performed Hi-C on the coral symbiont *Breviolum minutum*. We generated multi-

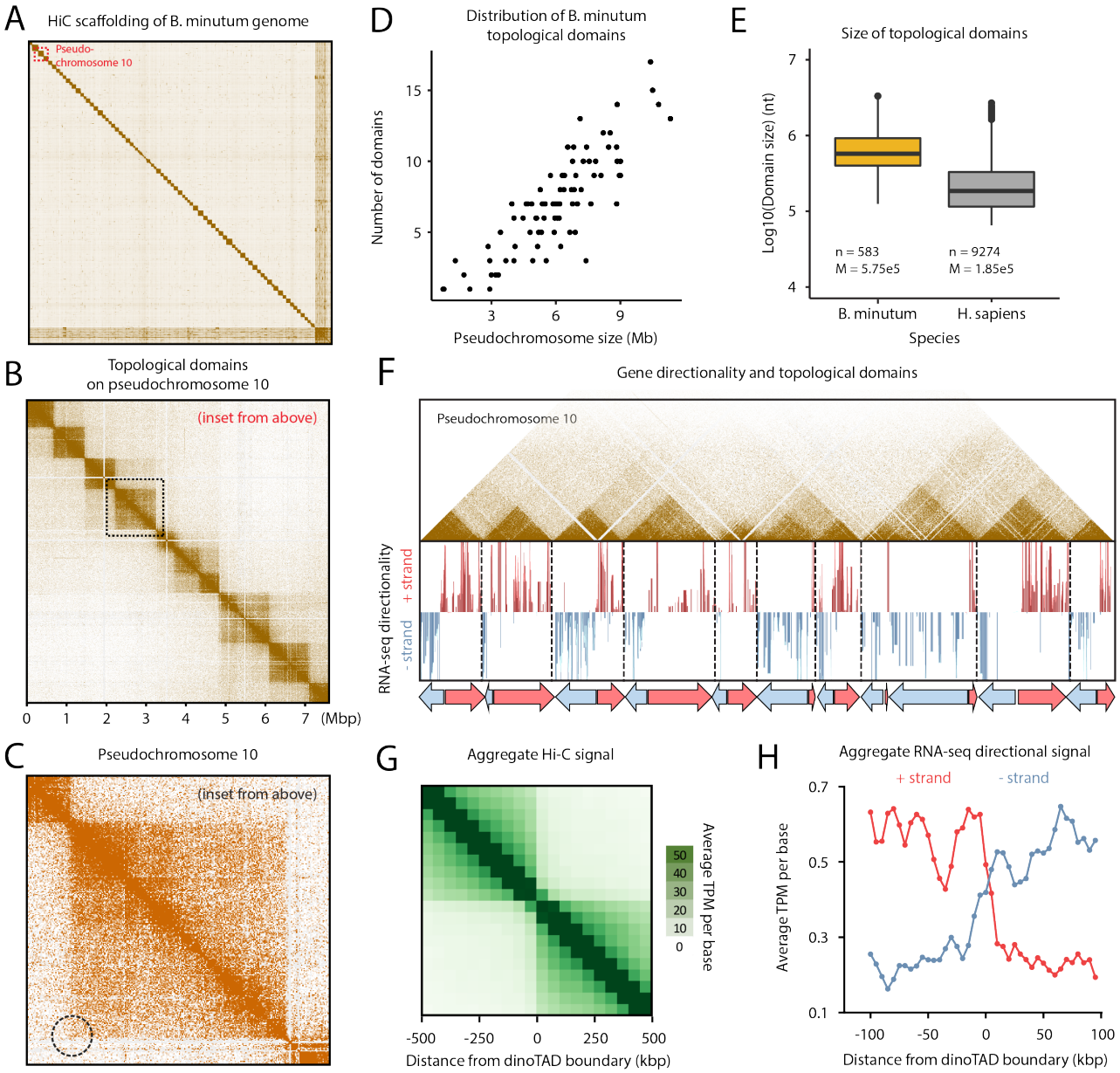

Figure 1: *B. minutum* genome is physically partitioned into dinoTADs defined by polycistronic gene arrays. (A) Hi-C scaffolding of the *B. minutum* draft genome assembly. (B) Inset from (A). KR-normalized 5-kb resolution Hi-C map for pseudochromosome 10. (C) Inset from (B). Hi-C loops and stripes are not observed in dinoTADs. (D) Scales of chromosome size with dinoTAD number. (E) Comparison of human and *B. minutum* topological domain sizes. (F) Hi-C map for pseudochromosome 10 together with forward- and reverse-strand transcript levels and gene arrays. (G) Average Hi-C contacts across dinoTAD boundaries. (H) Average forward- and reverse-strand RNA-seq levels across dinoTAD boundaries.

ple libraries under standard growth conditions and for cells grown at elevated temperature, obtaining ∼150–220 million Hi-C contacts for each (Supplementary Table 1). We pooled these libraries to generate a chromosome-level scaffolding of the previously fragmented *B. minutum* assembly[6]. We identified 91 major pseudochromosomes (≥ 500 kbp), encompassing ∼94% of the total sequence (Fig. 1A-B; Supplementary Fig. 1A), the longest being ∼11 Mbp in size, with a median length of 6.7 Mbp (Supplementary Fig. 1A). At 1-Mbp resolution, they exhibit a bipartite (occasionally tripartite) structure (Supplementary Fig. 2).

High-resolution maps revealed very strong topological domains, ≤200–≥2 Mbp in size (Fig. 1B-E; Supplementary Fig. 3–12). In mammals, TAD boundaries are demarcated by CTCF sites blocking loop extrusion, reflected in Hi-C maps by chromatin loops and "stripes". We observe no loop

or stripe features in *B. minutum* (Fig. 1C), suggesting a different mechanism for the formation of dinoflagellate TADs, which we term "dinoTADs". DinoTAD number correlates with chromosome size (Fig. 1D), and they are considerably larger than mammalian TADs (Fig. 1E).

We next compared Hi-C maps to available annotation features. Remarkably, we found that each dinoTAD corresponds to a pair of divergent gene arrays (Fig. 1F), and dinoTAD boundaries coincide with convergence between gene arrays (Fig. 1G-H).

The correspondence between dinoTADs and gene arrays suggested a role for transcription in their formation. Although TADs form independently of transcription in metazoan cells, transcription-induced self-interacting domains have been previously demonstrated in bacteria[8], and similar mechanisms have been proposed to explain some topological features in fission yeast[9]. This model makes a clear prediction – inhibition of transcription should result in dinoTADs decompaction.

To test this relationship, we first compared Hi-C maps for cells grown at 34 °C versus 27 °C, as heat stress could result in general transcription reduction[10]. We observed mild decompaction of dinoTADs at 34 °C, though domains remained intact (Supplementary Fig. 18–20).

We next carried out chemical transcription inhibition experiments. Since transcription inhibition conditions for *B. minutum* are not well established, we chose two inhibitors – triptolide and α-amanitin – with distinct mechanisms of action, and assayed multiple time points and doses (Fig. 2A-B). Amanitin directly inhibits RNA Polymerase II and is slow acting, while triptolide quickly blocks initiation by targeting the TFIIH XPB subunit[11]. However, the *B. minutum* XPB homolog is highly divergent[6], thus a moderate inhibition effect is not unexpected. Indeed, while we observed clear dose-dependent blurring of dinoTAD boundaries after triptolide treatment, broad dinoTAD-like structures remained (Fig. 2E-F; Supplementary Figures 25–28).

Strikingly, α-amanitin treatment resulted in a dose-dependent, progressive, near-complete dinoTAD decompaction (Fig. 2D,F; Supplementary Fig. 21–24). These effects were observed in both technical and biological replicates (Supplementary Fig. 21–24).

Of note, even at high doses, α-amanitin treatment did not detectably affect photosynthetic efficiency or cell viability relative to controls (Fig. 2C), excluding cell death as a confounding factor.

These experiments support a transcription-induced supercoiling model for dinoTAD formation. Torque generated by active polymerases produces positive/negative supercoiling ahead of/behind the transcription bubble. This can alter the twist of the double helix or induce superhelical writhe, which in turn can be accommodated through nucleosome remodeling, local alterations in DNA secondary structure, or formation of writhed structures such as plectonemes[12].

Although other topological constraints might also be involved, supercoiling-induced plectoneme formation over gene arrays is an intuitive mechanistic explanation for the presence of dinoTADs. An examination of dinoflagellate gene repertoires also corroborates this model, revealing a striking, dinoflagellate-specific expansion of topoisomerase II- and topoisomerase III-like genes (Fig. 1D; Supplementary Fig. 17; Supplementary Table 2), further suggestive of contending with increased levels of writhed forms of helical twist.

Comparison with self-interacting domains in bacteria or *S. pombe* shows much stronger topological insulation for dinoTADs (Supplementary Fig. 14) and 15)). Remarkably, no TAD domains are observed in kinetoplastids, the other lineage with long gene arrays and no transcriptional regulation (Supplementary Fig. 16).

These differences are readily explained by the unusual dinoflagellate properties. First, neither bacteria nor yeast possess comparably long gene arrays and transcription in those species is highly nonuniform; less transcription-induced torsional stress is therefore expected. Nucleosome loss is the second, and most salient difference. Single mammalian genes as long as dinoTADs are quite common, yet supercoiling is not apparent in mammalian Hi-C maps, nor is it seen in kinetoplastids, which have gene arrays but also have conventional chromatin. We therefore hypothesize that plectonemic structures form due to transcription-induced supercoiling in the nucleosome-depleted genomes of dinoflagellates, while in other eukaryotes, a combination of the wrapping of DNA around nucleosomes, interactions between nucleosomes, and accumulation of DNA twist, prevent their formation (Fig. 2H).

These results generate a number of open questions. How exactly are boundaries between dinoTADs formed mechanistically? Specific boundary elements of markedly different chromatin state could exist; alternatively, these boundaries may self-organize purely through torsion-related mechanisms. The roles that dinoflagellates' divergent histone genes play is also not clear. Finally, the relationship between Hi-C features and the "toroidal chromonemas"[13] observed by electron microscopy remains unknown. Answers to these questions, together with the dissection of specific roles different topoisomerase classes, will help fully elucidate the interplay between packaging proteins, transcription-induced torsional stress, and genome folding in dinoflagellates.

These observations also identify transcription-induced torsional stress as a key direction of future studies in eukaryotes generally. The strength of dinoTADs underlines the potency of this fundamental biological process for generating topological structure. The precise manner by which torsion is accommodated as twist and writhe, as well as its consequences for regulatory protein occupancy, transcriptional activity, and other chromatin processes, such as the behavior of ATP-dependent chromatin remodelers, are exciting questions remaining to be unraveled.

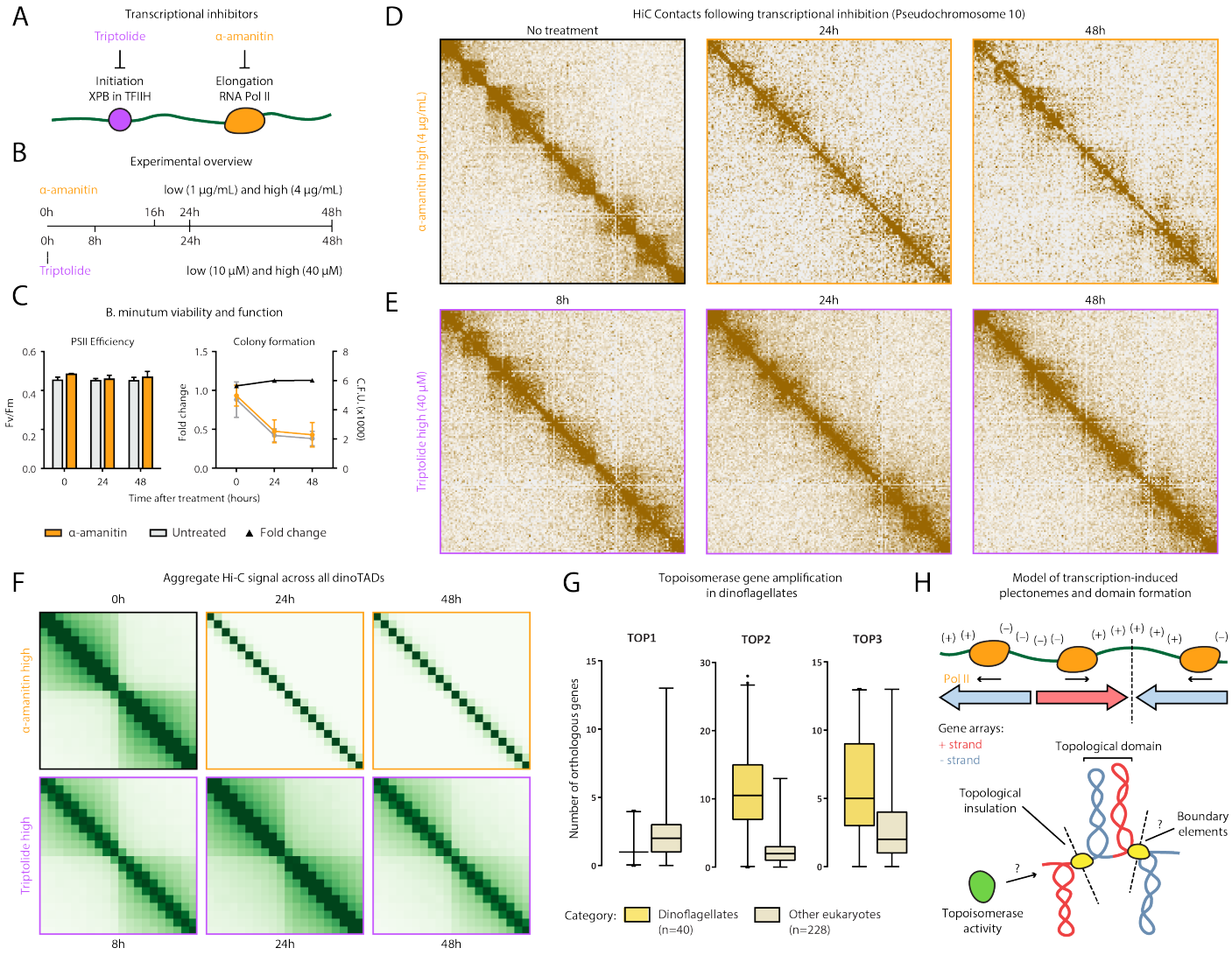

Figure 2: Decompaction of dinoTADs upon transcriptional inhibition and the transcription-induced supercoiling model for their formation. Shown is pseudochromosome 10. (A-B) Outline of transcription inhibition time course experiments. (C) Comparison of cell function, measured by PSII photosythetic efficiency, and cell viability, measured by colony formation (right), between α-amanitin-treated and untreated cells. (D) KR-normalized Hi-C maps (50-kb resolution) show marked loss of dinoTADs after α-amanitin treatment. (E) Hi-C maps show reduction of insulation at dinoTAD boundaries after triptolide treatment. (F) Metaplots of Hi-C signal around domain boundaries (50-kb resolution). (G) Amplification of *TOP2* and *TOP3* topoisomerases in dinoflagellates (based on MMETSP[7] transcriptome assemblies). (H) Transcription-induced supercoiling as driver of dinoflagellate chromatin folding. Transcribing polymerases introduce negative/positive DNA supercoiling behind/ahead of the transcription machinery. Interactions within supercoiled domains could explain the physical association of divergently-oriented arrays. Topological insulation could be driven by supercoiling-related effects, or by specific boundary elements. The exact role of the expanded repertoire of topoisomerases is also currently unclear.

Author contributions

G.K.M. performed Hi-C experiments. G.K.M and A.E.T. analyzed the data. A.E.T. and T.X. designed and carried out transcription inhibition experiments and cell viability experiments. T.X. carried out *S. minutum* culture and heat stress treatment. W.J.G., A.R.G.. A.K. and J.R.P. supervised the study. G.K.M., A.E.T. and T.X. interpreted data and wrote manuscript with input from all authors.

Acknowledgments

This work was supported by NIH grants (P50HG007735, RO1 HG008140, U19AI057266 and UM1HG009442

to W.J.G., 1UM1HG009436 to W.J.G. and A.K., 1DP2OD022870-01 and 1U01HG009431 to A.K.), the Rita Allen Foundation (to W.J.G.), the Baxter Foundation Faculty Scholar Grant, and the Human Frontiers Science Program grant RGY006S (to W.J.G). W.J.G is a Chan Zuckerberg Biohub investigator and acknowledges grants 2017-174468 and 2018-182817 from the Chan Zuckerberg Initiative. Fellowship support provided by the Stanford School of Medicine Dean's Fellowship (G.K.M.), the Siebel Scholars, the Enhancing Diversity in Graduate Education Program and the Weiland Family Fellowship (A.E.T.). This work is also supported by NSF-IOS EDGE Award 1645164 and Carnegie Venture grant 10907 (to T.X. and G.K.M.).

The authors would like to thank Zohar Shipony, Erez Lieberman Aiden, Philip Cleves, and members of the Greenleaf, Kundaje, Pringle and Grossman labs for helpful discussion and suggestions regarding this work.

References

1. Szabo Q, Bantignies F, Cavalli G. 2019. Principles of genome folding into topologically associating domains. *Sci Adv* **5**(4):eaaw1668.
2. Hackett JD, Anderson DM, Erdner DL, Bhattacharya D. 2004. Dinoflagellates: a remarkable evolutionary experiment. *Am J Bot* **91**:1523–1534.
3. Postberg J, Forcob S, Chang WJ, Lipps HJ. 2010. The evolutionary history of histone H3 suggests a deep eukaryotic root of chromatin modifying mechanisms. *BMC Evol Biol* **10**:259.
4. Marinov GK, Lynch M. 2015. Diversity and Divergence of Dinoflagellate Histone Proteins. *G3 (Bethesda)* **6**(2):397–422.
5. Janouškovec J, Gavelis GS, Burki F, Dinh D, Bachvaroff TR, Gornik SG, Bright KJ, Imanian B, Strom SL, Delwiche CF, Waller RF, Fensome RA, Leander BS, Rohwer FL, Saldarriaga JF. 2017. Major transitions in dinoflagellate evolution unveiled by phylotranscriptomics. *Proc Natl Acad Sci U S A* **114**(2):E171–E180.
6. Shoguchi E, Shinzato C, Kawashima T, Gyoja F, Mungpakdee S, Koyanagi R, Takeuchi T, Hisata K, Tanaka M, Fujiwara M, Hamada M, Seidi A, Fujie M, Usami T, Goto H, Yamasaki S, Arakaki N, Suzuki Y, Sugano S, Toyoda A, Kuroki Y, Fujiyama A, Medina M, Coffroth MA, Bhattacharya D, Satoh N. 2013. Draft assembly of the *Symbiodinium minutum* nuclear genome reveals dinoflagellate gene structure. *Curr Biol* **23**(15):1399–1408.
7. Keeling PJ, Burki F, Wilcox HM, Allam B, Allen EE, Amaral-Zettler LA, Armbrust EV, Archibald JM, Bharti AK, Bell CJ, Beszteri B, Bidle KD, Cameron CT, Campbell L, Caron DA, Cattolico RA, Collier JL, Coyne K, Davy SK, Deschamps P, Dyhrman ST, Edvardsen B, Gates RD, Gobler CJ, Greenwood SJ, Guida SM, Jacobi JL, Jakobsen KS, James ER, Jenkins B, John U, Johnson MD, Juhl AR, Kamp A, Katz LA, Kiene R, Kudryavtsev A, Leander BS, Lin S, Lovejoy C, Lynn D, Marchetti A, McManus G, Nedelcu AM, Menden-Deuer S, Miceli C, Mock T, Montresor M, Moran MA, Murray S, Nadathur G, Nagai S, Ngam PB, Palenik B, Pawlowski J, Petroni G, Piganeau G, Posewitz MC, Rengefors K, Romano G, Rumpho ME, Rynearson T, Schilling KB, Schroeder DC, Simpson AG, Slamovits CH, Smith DR, Smith GJ, Smith SR, Sosik HM, Stief P, Theriot E, Twary SN, Umale PE, Vaulot D, Wawrik B, Wheeler GL, Wilson WH, Xu Y, Zingone A, Worden AZ. 2014. The Marine Microbial Eukaryote Transcriptome Sequencing Project (MMETSP): illuminating the functional diversity of eukaryotic life in the oceans through transcriptome sequencing. *PLoS Biol* **12**(6):e1001889.
8. Le TB, Imakaev MV, Mirny LA, Laub MT. 2013. High-resolution mapping of the spatial organization of a bacterial chromosome. *Science* **342**(6159):731–734.
9. Benedetti F, Racko D, Dorier J, Burnier Y, Stasiak A. 2017. Transcription-induced supercoiling explains formation of self-interacting chromatin domains in *S. pombe*. *Nucleic Acids Res* **45**(17):9850–9859.
10. Levin RA, Beltran VH, Hill R, Kjelleberg S, McDougald D, Steinberg PD, van Oppen MJ. 2016. Sex, Scavengers, and Chaperones: Transcriptome Secrets of Divergent Symbiodinium Thermal Tolerances. *Mol Biol Evol* **33**(9):2201–2215.
11. Bensaude O. 2011. Inhibiting eukaryotic transcription: Which compound to choose? How to evaluate its activity? *Transcription* **2**(3):103–108.
12. Teves SS, Henikoff S. 2014. DNA torsion as a feedback mediator of transcription and chromatin dynamics. *Nucleus* **5**(3):211–218.
13. Oakley BR. Dodge JD. 1979. Evidence for a double-helically coiled toroidal chromonema in the dinoflagellate chromosome. *Chromosoma* **70**:277–291.
14. Xiang T, Hambleton EA, DeNofrio JC, Pringle JR, Grossman AR. 2013. Isolation of clonal axenic strains of the symbiotic dinoflagellate *Symbiodinium* and their growth and host specificity. *J Phycol* **49**(3):447–458.
15. Xiang T, Nelson W, Rodriguez J, Tolleter D, Grossman AR. 2015. *Symbiodinium* transcriptome and global responses of cells to immediate changes in light intensity when grown under autotrophic or mixotrophic conditions. *Plant J* **82**(1):67–80.
16. Rao SS, Huntley MH, Durand NC, Stamenova EK, Bochkov ID, Robinson JT, Sanborn AL, Machol I, Omer AD, Lander ES, Aiden EL. 2014. A 3D map of the human genome at kilobase resolution reveals principles of chromatin looping. *Cell* **159**(7):1665–1680.
17. Durand NC, Shamim MS, Machol I, Rao SS, Huntley MH, Lander ES, Aiden EL. 2016. Juicer Provides a One-Click System for Analyzing Loop-Resolution Hi-C Experiments. *Cell Syst* **3**(1):95–98.
18. Dudchenko O, Batra SS, Omer AD, Nyquist SK,

Hoeger M, Durand NC, Shamim MS, Machol I, Lander ES, Aiden AP, Aiden EL. 2017. De novo assembly of the Aedes aegypti genome using Hi-C yields chromosome-length scaffolds. *Science* **356**(6333):92–95.

19. Ramírez F, Bhardwaj V, Arrigoni L, Lam KC, Grüning BA, Villaveces J, Habermann B, Akhtar A, Manke T. 2018. High-resolution TADs reveal DNA sequences underlying genome organization in flies. *Nat Commun* **9**(1):189.
20. Dobin A, Davis CA, Schlesinger F, Drenkow J, Zaleski C, Jha S, Batut P, Chaisson M, Gingeras TR. 2013. STAR: ultrafast universal RNA-seq aligner. *Bioinformatics* **29**(1):15–21.
21. Pertea M, Pertea GM, Antonescu CM, Chang TC, Mendell JT, Salzberg SL. 2015. StringTie enables improved reconstruction of a transcriptome from RNA-seq reads. *Nat Biotechnol* **33**(3):290-295.
22. Eddy SR. 2011. Accelerated Profile HMM Searches. *PLoS Comput Biol* **7**(10):e1002195.
23. Finn RD, Bateman A, Clements J, Coggill P, Eberhardt RY, Eddy SR, Heger A, Hetherington K, Holm L, Mistry J, Sonnhammer EL, Tate J, Punta M. 2014. Pfam: the protein families database. *Nucleic Acids Res* **42**(Database issue):D222–230.
24. Knight P, Ruiz D. 2013. A fast algorithm for matrix balancing. *IMA J Num Anal* **33**(3):1029–1047.

Supplementary Materials

Supplementary Methods

Except where otherwise stated, computational analyses were carried out using custom-written Python scripts.

B. minutum cell culture

The clonal axenic *Symbiodinium/Breviolum minutum* strain SSB01 was used in all experiments. Stock cultures were grown as previously described[14,15] in Daigo's IMK medium for marine microalgae (Wako Pure Chemicals) supplemented with casein hydrolysate (IMK+Cas) at 27 °C at a light intensity of 10 μmol photons m^2 s^1 from Philips ALTO II 25-W bulbs on a 12-h-light:12-h-dark cycle. The medium was prepared in artificial seawater (ASW).

Transcription inhibition experiments

For α-amanitin treatment, *Breviolum minutum* cells at a density of $\sim$1 $\times 10^6$ cells/mL were treated with α-amanitin (Sigma-Aldrich, Cat # A2263) at concentrations of 1 μg/mL ("normal" dose) and 4 μg/mL ("high") dose.

Samples were harvested at 0, 24, and 48 hours after treatment.

For triptolide treatment, *Breviolum minutum* cells at a density of $\sim$1 $\times 10^6$ cells/mL were treated with triptolide (Sigma-Aldrich, Cat # T3652) at concentrations of 10 μM ("normal" dose) and 40 μM ("high") dose.

Samples were harvested fat 0, 8, 24 and 48 hours after treatment.

Cell viability measurements

Photosynthetic activity

Maximum quantum yields of photosystem II, $Fv/Fm = (Fm - F0)/Fm$ was used to indicate photosynthetic function. S. minutum cultures (approximately 10^6 cells/mL) were collected and dark adapted for 5 min, and Fv/Fm was determined using a Dual Pam-100 fluorometer (Heinz Walz).

Colony formation assay

Fresh SSB01 cells were sampled at 0, 24 and 48 hours after the treatment of transcription inhibitor α-amanitin. For each condition, cell suspensions were diluted 1:5 and 1:10 before plating 1 μL of each dilution on marine broth (BD) agar plates. Plates were incubated at 27 °C at a light intensity of 10 μmol photons m^2 s^1. Cell numbers on each plate were counted after three weeks.

Hi-C experiments

The in situ Hi-C procedure used to map 3D genomic interactions in *Symbiodinium* was adapted from previous studies[16] as follows:

Symbiodinium minutum SSBO1 cells were first crosslinked using 37% formaldehyde (Sigma) at a final concentration of 1% for 15 minutes at room temperature. Formaldehyde was then quenched using 2.5 M Glycine at a final concentration of 0.25 M. Cells were subsequently centrifuged at 2,000 g for 5 minutes, washed once in 1× PBS, and stored at -80 °C.

Cell lysis was initiated by incubation with 250 μL of cold Hi-C Lysis Buffer (10 mM Tris-HCl pH 8.0, 10 mM NaCl, 0.2% Igepal CA630) on ice for 15 minutes, followed by centrifugation at 2,500 g for 5 minutes, a wash with 500 μL of cold Hi-C Lysis Buffer, and centrifugation at 2,500 g for 5 minutes. The pellet was the resuspended in 50 μL of 0.5% SDS and incubated at 62 °C for 10 minutes. SDS was quenched by adding 145 μL of H_2O and 25 μL of 10% Triton X-100 and incubating at 37 °C for 15 minutes.

Restriction digestion was carried out by adding 25 μL of 10× NEBuffer 2 and 100 U of the MboI restriction enzyme (NEB, R0147) and incubating for $\geq$2 hours at 37 °C in a Thermomixer at 900 rpm. The reaction was then incubated at 62 °C for 20 minutes in order to inactivate the restriction enzyme.

Fragment ends were filled in by adding 37.5 μL of 0.4 mM biotin-14-dATP (ThermoFisher Scientific, # 19524-016), 1.5 μL each of 10 mM dCTP, dGTP and dTTP, and 8 μL of 5U/μL DNA Polymerase I Large (Klenow) Fragment (NEB M0210). The reaction was the incubated at 37 °C in a Thermomixer at 900 rpm for 45 minutes.

Fragment end ligation was carried out by adding 663 μL H_2O, 120 μL 10× NEB T4 DNA ligase buffer (NEB B0202), 100 μL of 10% Triton X-100, 12 μL of 10 mg/mL Bovine Serum Albumin (100× BSA, NEB), 5 μL of 400 U/μL T4 DNA Ligase (NEB M0202), and incubating at room temperature for $\geq$4 hours with rotation.

Nuclei were then pelleted by centrifugation at 3,500 g for 5 minutes; the pellet was resuspended in 200 μL ChIP Elution Buffer (1% SDS, 0.1 M $NaHCO_3$), Proteinase K was added, and incubated at 65 °C overnight to reverse crosslinks.

After addition of 600 μL 1×TE buffer, DNA was sonicated using a Qsonica S-4000 with a 1/16" tip for 3 minutes, with 10 second pulses at intensity 3.5, and 20 seconds rest between pulses. DNA was then purified using the MinElute PCR Purificaiton Kit (Qiagen #28006), with elution in a total volume of 300 μL 1× EB buffer.

For streptavidin pulldown of biotin-labeled DNA, 150

μL of 10 mg/mL Dynabeads MyOne Streptavidin T1 beads (Life Technologies, 65602) were separated on a magnetic stand, then washed with 400 μL of 1× TWB (Tween Washing Buffer; 5 mM Tris-HCl pH 7.5; 0.5 mM EDTA; 1 M NaCl; 0.05% Tween 20). The beads were resuspended in 300 μL of 2× Binding Buffer (10 mM Tris-HCl pH 7.5, 1 mM EDTA; 2 M NaCl), the sonicated DNA was added, and the beads were incubated for ≥15 minutes at room temperature on a rotator. After separation on a magnetic stand, the beads were washed with 600 μL of 1× TWB, and heated at 55 °C in a Thermomixer with shaking for 2 minutes. After removal of the supernatant on a magnetic stand, the TWB wash and 55 °C incubation were repeated.

Final libraries were prepared on beads using the NEBNext Ultra II DNA Library Prep Kit (NEB, #E7645) as follows. End repair was carried out by resuspending beads in 50 μL 1× EB buffer, and adding 3 μL NEB Ultra End Repair Enzyme and 7 μL NEB Ultra End Repair Enzyme, followed by incubation at 20 °C for 30 minutes and then at 65 °C for 30 minutes.

Adapters were ligated to DNA fragments by adding 30 μL Blunt Ligation mix, 1 μL Ligation Enhancer and 2.5 μL NEB Adapter, incubating at 20 °C for 20 minutes, adding 3 μL USER enzyme, and incubating at 37 °C for 15 minutes.

Beads were then separated on a magnetic stand, and washed with 600 μL TWB for 2 minutes at 55 °C, 1000 rpm in a Thermomixer. After separation on a magnetic stand, beads were washed in 100 μL 0.1 × TE buffer, then resuspended in 16 μL 0.1 × TE buffer, and heated at 98 °C for 10 minutes.

For PCR, 5 μL of each of the i5 and i7 NEB Next sequencing adapters were added together with 25 μL 2× NEB Ultra PCR Mater Mix. PCR was carried out with a 98 °C incubation for 30 seconds and 12 cycles of 98 °C for 10 seconds, 65 °C for 30 seconds, and 72 °C for 1 minute, followed by incubation at 72 °C for 5 minutes.

Beads were separated on a magnetic stand, and the supernatant was cleaned up using 1× AMPure XP beads.

Libraries were sequenced in a paired-end format on a Illumina NextSeq instrument using NextSeq 500/550 high output kits (either 2×75 or 2×36 cycles).

Hi-C data processing and assembly scaffolding

As an initial step, Hi-C sequencing reads from all libraries were trimmed of adapter sequences, pooled together, and processed against the previously published *B. minutum* assembly[6] using the Juicer pipeline[17] for analyzing Hi-C datasets (version 1.8.9 of Juicer Tools).

The resulting Hi-C matrices were then used as input to the 3D DNA pipeline[18] for automated scaffolding with the following parameters: `--editor-coarse-resolution 5000 --editor-coarse-region 5000 --polisher-input-size 100000 --polisher-coarse-resolution 1000 --polisher-coarse-region 300000 --splitter-input-size 100000 --splitter-coarse-resolution 5000 --splitter-coarse-region 300000 --sort-output --build-gapped-map -r 10 -i 5000`.

Manual correction of obvious assembly and scaffolding errors was then carried out using Juicebox[17].

After finalizing the scaffolding, Hi-C reads were reprocessed against the new assembly using the Juicer pipeline. This was done individually for each library as well as together for the pooled set of reads.

Data was extracted from the final read matrices using the Juicer suite of tools for Hi-C data analysis.

Identification of Hi-C domains

Hi-C matrices were first converted to *cool* format using HiCExplorer[19] "`hicConvertFormat`" with parameters `--inputFormat hic --outputFormat h5` and default resolutions. Subsequent HiCExplorer commands were carried out at 10 kb, 25 kb, and 50 kb resolutions with similar results. Matrices were normalized using "`hicNormalize`" with parameter `--normalize smallest`, and corrected using "`hicCorrectMatrix correct`" with parameters `--correctionMethod KR`. Hi-C domains were computationally identified using the "`hicFindTADs`" from HiCExplorer with parameter `--correctForMultipleTesting fdr`.

RNA-seq datasets

Approximately 5×10^7 cells were collected by centrifugation at 100 *g* for 5 minutes at room temperature. Total RNA was extracted and libraries were constructed for RNA-Seq using the TruSeq RNA Library Prep Kit V2 (Illumina, San Diego, CA, USA) according to the manufacturer protocol. All of the raw sequencing reads are available at Sequence Read Archive (SRA) with accession number SRX7258938.

RNA-seq data analysis

RNA-seq reads were aligned against the corresponding assemblies using the STAR aligner[20] (version 2.5.3a) with the following settings: `--limitSjdbInsertNsj 10000000 --outFilterMultimapNmax 50 \verb–outFilterMismatchNmax— 999 --outFilterMismatchNoverReadLmax 0.04 --alignIntronMin 10 --alignIntronMax 1000000 --alignMatesGapMax 1000000 --alignSJoverhangMin 8 --alignSJDBoverhangMin 1 --sjdbScore 1 --twopassMode Basic --twopass1readsN -1`. As available RNA-seq datasets for *B. minutum* are not strand-specific, the strand orientation of the transcriptome was visualized as follows. Aligned reads were first *de novo* assembled into transcripts and quantified at the transcript level using Stringtie[21] (version 1.3.3.b); the orientation of splice junctions serves as a reliable guide for the directionality of these transcripts. Open reading frames (ORFs) were identified for each transcript, and transcripts with ORFs shorter than 60 amino acids were filtered out of the transcript set. Strand-specific genomic tracks were then generated

by assigning to each basepair covered by at least one exon in that set the sum of the TPM (Transcript Per Million transcripts) values of all transcripts it is included in.

External Hi-C datasets

Hi-C data for *Trypanosoma brucei* was obtained from GEO accession GSE118764.

Hi-C data for *Schizosaccharomyces pombe* was obtained from GEO accession GSE57316.

Hi-C data for *Caulobacter vibrioides* CB15 was obtained from GEO accession GSE45966.

Sequence Analysis

Topoisomerase and other replication-related proteins were identified in annotated MMETSP transcriptome assemblies using HMMER3.0[22] and the Pfam 27.0 protein domain database[23] as previously described[4].

Supplementary Tables

Supplementary Table 1: Summary of Hi-C datasets used in this study

Hi-C library	Number raw read pairs	Estimated library complexity	Number Hi-C contacts
L142-SSBO1-HIC	534,609,924	920,112,029	220,908,462
L533-SSBO1_27C_Hi-C	556,089,015	1,513,268,498	151,618,419
L534-SSBO1_34C_Hi-C	531,461,453	2,971,291,849	165,231,965
L1240-SSBO1-α_amanitin-0h-Hi-C	111,333,226	233,525,989	34,384,671
L1241-SSB01-α_amanitin-16h-Hi-C-rep1	60,696,609	317,650,525	24,238,281
L1242-SSB01-α_amanitin-16h-Hi-C-rep2	67,376,168	227,736,960	25,551,603
L1243-SSB01-α_amanitin-24h-Hi-C-rep1	81,532,584	235,898,386	29,748,439
L1244-SSB01-α_amanitin-24h-Hi-C-rep2	106,381,220	110,607,925	28,845,306
L1245-SSB01-α_amanitin-48h-Hi-C-rep1	90,180,763	155,046,434	27,045,343
L1246-SSB01-α_amanitin-48h-Hi-C-rep2	78,982,528	152,703,652	22,153,117
L1247-SSB01-α_amanitin_high-48h-Hi-C	110,015,013	157,350,902	28,138,017
L1332-SSB01-α_amanitin-0h-Hi-C-technical_rep	117,543,007	182,213,300	34,089,285
L1333-SSB01-α_amanitin-48h-Hi-C-rep1-technical_rep	117,821,773	82,740,021	23,654,760
L1334-SSB01-α_amanitin_high-48h-Hi-C-technical_rep	95,662,202	164,149,035	23,944,231
L1336-SSB01-α_amanitin_high-24h-Hi-C-second_time_course	58,747,402	103,174,104	15,663,160
L1337-SSB01-α_amanitin_high-48h-Hi-C-second_time_course	83,691,617	62,658,394	14,523,464
L1344-SSB01-α_amanitin/triptolide_0h_NT-Hi-C	79,383,186	208,157,102	23,592,335
L1346-SSB01-triptolide_8h_normal_dose-Hi-C	81,731,190	193,514,340	22,700,096
L1347-SSB01-triptolide_8h_high_dose-Hi-C	112,753,865	187,235,670	28,552,855
L1348-SSB01-Triptolide_24h NT-Hi-C	52,148,987	166,057,825	15,674,551
L1349-SSB01-triptolide_24h_normal_dose-Hi-C	132,715,807	206,778,720	36,745,591
L1350-SSB01-triptolide_24h_high_dose-Hi-C	98,429,444	265,027,975	32,121,298
L1351-SSB01-Triptolide_48h NT-Hi-C	96,846,551	240,797,245	28,296,251
L1352-SSB01-triptolide_48h_normal_dose-Hi-C	85,347,611	255,500,603	25,051,605
L1353-SSB01-triptolide_48h_high_dose-Hi-C	99,978,207	215,504,692	26,572,806

Supplementary Table 2: Inventory of topoisomerases and some other proteins involved in DNA replication in dinoflagellates and other eukaryotes as annotated by transcriptome assemblies in the MMETSP databses

clade	species	TOP1	TOP2	TOP3	MCM	PCNA	RPA1	RPA2	RPA3	RFC1
Amoebozoa	*Stereomyxa ramosa* Chinc5	1	2	2	6	2	3	0	2	1
Amoebozoa	*Vexillifera* sp. DIVA3 564 2	1	2	2	7	1	2	0	0	1
Apicomplexa	*Lankesteria abbottii* Grappler Inlet BC	1	1	0	12	5	1	0	0	1
Bicosoecid	Bicosoecid sp ms1	1	0	0	3	1	1	1	1	0
Bicosoecid	*Cafeteria roenbergensis* E4 10	1	0	2	6	1	0	0	1	0
Bicosoecid	*Cafeteria* sp. Caron Lab Isolate	1	1	4	15	1	1	0	1	1
Bolidophyte	*Bolidomonas pacifica* CCMP 1866	2	5	7	8	1	1	0	0	1
Chlorarachniophyte	*Bigelowiella natans* CCMP1258.1	1	1	9	3	1	4	1	0	0
Chlorarachniophyte	*Bigelowiella natans* CCMP1259	1	1	6	7	1	4	1	0	1
Chlorarachniophyte	*Bigelowiella natans* CCMP 2755	0	0	4	5	1	4	1	0	1
Chlorarachniophyte	*Bigelowiella natans* CCMP623	1	3	7	9	1	2	1	0	1
Chlorarachniophyte	*Chlorarachnion reptans* CCCM449	2	4	8	11	2	3	1	0	1
Chlorarachniophyte	*Lotharella amoebiformis* CCMP2058	2	6	5	10	1	4	1	0	1
Chlorarachniophyte	*Lotharella globosa* CCCM811	1	2	1	0	1	1	1	1	1
Chlorarachniophyte	*Lotharella oceanica* CCMP622	1	0	0	1	1	2	1	1	1
Chlorarachniophyte	*Norrisiella sphaerica* BC52	1	0	3	0	1	2	1	1	0
Chlorarachniophyte	*Partenskyella glossopodia* RCC365	1	2	1	7	1	3	1	2	1
Chlorophyte	*Bathycoccus prasinos* CCMP1898	1	2	3	9	1	2	0	0	0
Chlorophyte	*Bathycoccus prasinos* RCC716	1	2	3	7	1	3	0	0	1
Chlorophyte	*Chlamydomonas* cf sp CCMP681	1	0	0	5	2	1	0	0	1
Chlorophyte	*Crustomastix stigmata* CCMP3273	1	2	4	10	1	1	1	0	1
Chlorophyte	*Cyanoptyche gloeocystis* SAG4.97	1	0	0	4	1	1	1	0	0
Chlorophyte	*Dolichomastix tenuilepis* CCMP3274	1	1	3	1	2	1	0	1	1
Chlorophyte	*Dunaliella tertiolecta* CCMP1320	1	2	3	10	1	2	0	1	1
Chlorophyte	*Mantoniella antarctica* SL 175	1	8	4	13	1	2	2	1	1
Chlorophyte	*Mantoniella* sp CCMP1436	1	2	1	2	1	1	1	1	1
Chlorophyte	*Micromonas* sp CCMP2099	1	2	2	9	1	2	0	1	1
Chlorophyte	*Micromonas* sp NEPCC29	1	2	3	7	1	2	0	1	1
Chlorophyte	*Micromonas* sp RCC472	1	2	2	7	1	2	1	0	1
Chlorophyte	*Nephroselmis pyriformis* CCMP717	1	4	8	10	1	2	0	1	1
Chlorophyte	*Picochlorum oklahomensis* CCMP2329	1	2	2	6	2	2	1	0	1
Chlorophyte	*Picochlorum* sp. RCC944	1	1	2	6	1	2	0	2	1
Chlorophyte	*Picocystis salinarum* CCMP1897	1	2	1	8	2	2	1	2	1
Chlorophyte	*Polytomella parva* SAG 63 3	1	5	3	18	2	3	0	0	1
Chlorophyte	*Prasinoderma coloniale* CCMP1413	1	2	0	2	1	1	0	0	0
Chlorophyte	*Prasinoderma singularis* RCC927	1	1	1	7	1	1	0	1	1
Chlorophyte	*Pterosperma* sp. CCMP1384	1	0	0	3	1	1	1	1	1
Chlorophyte	*Pycnococcus provasolii* RCC2336	1	1	0	9	1	1	0	0	1
Chlorophyte	*Pycnococcus provasolii* RCC931	1	0	0	7	1	1	0	0	1
Chlorophyte	*Pyramimonas parkeae* CCMP726	1	0	4	7	1	2	1	1	1
Chlorophyte	*Stichococcus* sp RCC1054	1	1	1	8	1	1	0	0	1
Chlorophyte	*Tetraselmis chuii* PLY429	2	0	0	0	0	2	0	1	2
Chlorophyte	*Tetraselmis striata* LANL1001	1	4	4	11	1	2	0	1	1
Choanoflagellata	*Acanthoeca* like sp 10tr	1	3	4	10	1	1	0	1	1
Chromerida	*Chromera velia* CCMP2878	1	1	3	10	2	2	0	0	1
Chromerida	*Vitrella brassicaformis* CCMP3346	1	1	2	9	2	1	0	0	1
Chrysophyte	*Chromulina nebulosa* UTEXLB2642	1	1	1	2	1	1	0	0	1
Chrysophyte	*Dinobryon* sp UTEXLB2267	1	3	0	8	1	1	0	0	1
Chrysophyte	*Mallomonas* Sp CCMP3275	1	2	1	9	1	1	0	1	1
Chrysophyte	*Ochromonas* sp CCMP1393	1	2	2	7	1	1	0	0	1
Chrysophyte	*Paraphysomonas bandaiensis* Caron Lab Isolate	1	2	3	9	2	1	1	1	1
Chrysophyte	*Paraphysomonas imperforata* PA2	0	1	3	6	1	1	1	1	1
Chrysophyte	*Pelagococcus subviridis* CCMP1429	1	1	2	11	1	0	0	0	1
Chrysophyte	*Spumella elongata* CCAP 955 1	1	1	3	10	4	3	0	1	1
Ciliate	*Aristerostoma* sp. ATCC 50986	2	1	1	0	2	1	0	0	2
Ciliate	*Blepharisma japonicum* Stock R1072	0	0	0	7	4	1	0	0	0

Continued on next page

Supplementary Table 2 – *Continued from previous page*

clade	species	TOP1	TOP2	TOP3	MCM	PCNA	RPA1	RPA2	RPA3	RFC1
Ciliate	*Climacostomum virens* Stock W 24	1	2	2	9	3	1	0	0	3
Ciliate	*Condylostoma magnum* COL2	0	0	0	2	0	0	0	0	0
Ciliate	*Euplotes focardii* TN1	1	0	0	5	2	1	0	2	0
Ciliate	*Euplotes harpa* FSP1.4	2	0	5	3	1	0	0	1	0
Ciliate	*Fabrea salina* Unknown	1	1	3	7	2	3	0	0	2
Ciliate	*Favella taraikaensis* FeNarragansettBay	0	1	2	7	3	0	0	0	0
Ciliate	*Litonotus pictus* P1	1	1	2	0	0	0	0	0	0
Ciliate	*Mesodinium pulex* SPMC105	2	13	2	16	9	4	0	0	6
Ciliate	*Myrionecta rubra* CCMP2563	0	1	4	11	1	1	0	1	0
Ciliate	*Platyophrya macrostoma* WH	4	4	4	23	4	6	0	0	3
Ciliate	*Protocruzia adherens* Boccale	3	1	0	9	3	3	0	0	1
Ciliate	*Pseudokeronopsis* sp. OXSARD2	1	1	1	6	1	0	0	1	1
Ciliate	*Strombidinopsis acuminatum* SPMC142	2	6	0	32	10	5	0	0	0
Ciliate	*Strombidinopsis* sp. SopsisLIS2011	1	0	0	8	3	2	0	0	0
Ciliate	*Strombidium* inclinatum S3	1	1	2	8	1	1	0	0	1
Ciliate	*Strombidium rassoulzadegani* ras09	1	0	1	6	1	1	0	1	0
Ciliate	*Tiarina fusus* LIS	1	7	3	16	3	4	2	1	1
Cryptophyte	*Chroomonas mesostigmatica* cf CCMP1168	1	5	4	8	1	2	2	0	1
Cryptophyte	*Cryptomonas curvata* CCAP979 52	2	0	2	0	1	1	0	1	0
Cryptophyte	*Cryptomonas paramecium* CCAP977 2a	3	2	2	5	1	1	0	0	1
Cryptophyte	*Geminigera cryophila* CCMP2564	2	1	5	11	1	2	0	1	2
Cryptophyte	*Geminigera* sp. Caron Lab Isolate	1	3	5	18	1	5	0	1	1
Cryptophyte	*Goniomonas pacifica* CCMP1869	8	4	4	12	1	5	1	3	7
Cryptophyte	*Guillardia theta* CCMP 2712	1	0	2	3	1	1	0	1	0
Cryptophyte	*Hemiselmis andersenii* CCMP644	1	2	5	12	1	2	0	1	1
Cryptophyte	*Hemiselmis rufescens* PCC563	1	0	3	7	1	1	1	1	1
Cryptophyte	*Hemiselmis tepida* CCMP443	3	2	0	3	1	1	1	1	1
Cryptophyte	*Hemiselmis viresens* PCC157	1	0	0	7	1	1	0	1	0
Cryptophyte	*Palpitomonas bilix* NIES 2562	0	1	2	13	4	3	0	1	3
Cryptophyte	*Proteomonas sulcata* CCMP704	0	1	0	3	1	1	0	0	1
Cryptophyte	*Rhodomonas lens* RHODO	2	3	2	2	2	2	0	1	0
Cryptophyte	*Rhodomonas* sp. CCMP768	1	0	1	0	1	1	0	0	0
Diatome	*Amphiprora* sp.	1	4	3	9	1	1	0	0	1
Diatome	*Amphora coffeaeformis* CCMP127	1	1	0	4	1	1	0	0	0
Diatome	*Asterionellopsis glacialis* CCMP134	1	7	1	10	1	1	0	0	1
Diatome	*Astrosyne radiata* 13vi08 1A	1	8	3	6	3	2	0	0	1
Diatome	*Attheya septentrionalis* CCMP2084	1	2	0	9	1	1	0	0	1
Diatome	*Aulacoseira subarctica* CCAP 1002 5	1	2	3	8	2	1	0	0	1
Diatome	*Chaetoceros affinis* CCMP159	1	3	1	8	1	1	0	0	1
Diatome	*Chaetoceros curvisetus*	1	4	4	6	1	3	0	0	1
Diatome	*Chaetoceros debilis* MM31A_1	1	3	1	12	1	1	0	0	1
Diatome	*Chaetoceros neogracile* CCMP1317	1	9	3	10	1	1	0	1	1
Diatome	*Coscinodiscus wailesii* CCMP2513	1	3	6	10	1	1	0	1	1
Diatome	*Craspedostauros australis* CCMP3328	1	0	0	4	0	1	0	0	0
Diatome	*Cyclophora tenuis* ECT3854	1	1	0	3	1	1	0	0	0
Diatome	*Cyclotella meneghiniana* CCMP 338	1	4	3	8	1	1	0	0	1
Diatome	*Cylindrotheca closterium* KMMCC:B 181	3	7	3	14	1	2	0	0	1
Diatome	*Dactyliosolen fragilissimus* Unknown	1	3	3	8	1	1	0	1	1
Diatome	*Ditylum brightwellii* GSO103	1	4	3	11	1	1	0	1	1
Diatome	*Ditylum brightwellii* GSO104	1	4	5	10	1	1	0	1	1
Diatome	*Ditylum brightwellii* GSO105	1	2	3	11	2	1	0	1	1
Diatome	*Entomoneis* sp. CCMP2396	0	1	0	0	1	1	0	0	0
Diatome	*Eucampia antarctica* CCMP1452	1	3	0	5	1	1	1	1	1
Diatome	*Extubocellulus spinifer* CCMP396	1	4	10	13	2	5	3	1	2
Diatome	*Fragilariopsis kerguelensis* L2_C3	1	3	3	11	1	1	2	0	1
Diatome	*Fragilariopsis kerguelensis* L26_C5	1	3	5	22	1	1	3	0	1
Diatome	*Grammatophora oceanica* CCMP 410	1	1	3	5	1	1	0	0	1
Diatome	*Helicotheca tamensis* CCMP826	0	1	0	1	1	1	0	1	0
Diatome	*Leptocylindrus danicus* var. apora B651	3	5	3	0	3	2	0	1	1

Continued on next page

Supplementary Table 2 – *Continued from previous page*

clade	species	TOP1	TOP2	TOP3	MCM	PCNA	RPA1	RPA2	RPA3	RFC1
Diatome	*Leptocylindrus danicus* var. danicus B650	3	11	3	19	1	1	0	1	2
Diatome	*Licmophora paradoxa* CCMP2313	1	1	3	7	1	2	0	0	1
Diatome	*Minutocellus polymorphus* CCMP3303	0	0	0	3	1	1	1	1	0
Diatome	*Minutocellus polymorphus* NH13	2	8	7	21	1	0	1	0	3
Diatome	*Minutocellus polymorphus* RCC2270	1	2	1	7	1	1	1	1	1
Diatome	*Nitzschia punctata* CCMP561	1	2	2	9	1	1	1	1	1
Diatome	*Odontella aurita* isolate 1302 5	1	3	7	11	2	2	1	1	1
Diatome	*Odontella sinensis* Grunow 1884	1	3	0	2	1	1	1	1	1
Diatome	*Proboscia alata* PI_D3	1	7	2	21	1	1	2	0	1
Diatome	*Pseudo-nitzschia australis* 10249_10_AB	1	3	4	8	1	1	1	0	1
Diatome	*Pseudo-nitzschia fradulenta* WWA7	2	11	6	24	4	5	0	0	3
Diatome	*Rhizosolenia setigera* CCMP 1694	1	7	4	18	1	2	0	0	2
Diatome	*Skeletonema dohrnii* SkelB	1	2	0	14	1	1	2	1	1
Diatome	*Skeletonema marinoi* SkelA	1	1	2	7	1	1	2	0	1
Diatome	*Skeletonema menzelii* CCMP793	1	4	4	8	1	1	2	0	1
Diatome	*Stauroneis constricta* CCMP1120	1	0	1	1	1	1	1	0	0
Diatome	*Staurosira complex* sp. CCMP2646	1	3	4	8	1	1	0	1	1
Diatome	*Stephanopyxis turris* CCMP 815	2	0	1	7	3	2	0	1	1
Diatome	*Striatella unipunctata* CCMP2910	4	2	1	6	3	0	1	0	2
Diatome	*Synedropsis recta* cf CCMP1620	1	2	0	1	1	1	1	1	0
Diatome	*Thalassionema frauenfeldii* CCMP 1798	1	5	7	15	1	3	1	1	2
Diatome	*Thalassionema nitzschioides* L26_B	1	3	4	8	1	1	1	1	1
Diatome	*Thalassiosira antarctica* CCMP982	1	4	2	12	1	1	3	1	1
Diatome	*Thalassiosira gravida* GMp14c1	1	1	3	13	1	1	2	1	1
Diatome	*Thalassiosira miniscula* CCMP1093	1	13	6	10	1	1	2	1	1
Diatome	*Thalassiosira oceanica* CCMP1005	1	10	1	10	1	1	0	0	1
Diatome	*Thalassiosira rotula* CCMP3096	1	5	3	11	1	1	2	1	1
Diatome	*Thalassiosira rotula* GSO102	1	3	2	11	1	1	1	1	1
Diatome	*Thalassiosira weissflogii* CCMP1010	1	4	1	9	1	0	1	0	1
Diatome	*Thalassiosira weissflogii* CCMP1336	1	4	1	8	1	0	1	0	1
Diatome	*Thalassiothrix antarctica* L6_D1	1	2	4	6	1	1	0	1	1
Diatome	*Triceratium dubium* CCMP147	0	1	1	1	1	0	1	1	0
Dinoflagellata	*Alexandrium temarense* CCMP1771	3	18	12	45	18	10	3	4	2
Dinoflagellata	*Amphidinium carterae* CCMP1314	2	5	5	8	2	4	0	0	3
Dinoflagellata	*Azadinium spinosum* 3D9	1	12	13	35	11	6	0	0	3
Dinoflagellata	*Brandtodinium nutriculum* RCC3387	1	13	9	30	21	4	0	0	3
Dinoflagellata	*Ceratium fusus* PA161109	1	15	10	18	12	9	1	1	3
Dinoflagellata	*Crypthecodinium cohnii* Seligo	1	6	5	15	2	4	0	0	3
Dinoflagellata	*Dinophysis acuminata* DAEP01	4	15	9	29	13	8	0	0	2
Dinoflagellata	*Durinskia baltica* CSIRO_CS 38	2	12	9	18	9	8	0	0	4
Dinoflagellata	*Gambierdiscus australes* CAWD 149	1	5	0	9	14	6	0	0	2
Dinoflagellata	*Glenodinium foliaceum* CCAP1116_3	2	9	3	23	7	6	0	1	4
Dinoflagellata	*Gonyaulax spinifera* CCMP409	1	2	0	10	10	8	1	1	1
Dinoflagellata	*Heterocapsa rotundata* SCCAP K 0483	2	19	4	12	6	4	0	0	6
Dinoflagellata	*Heterocapsa triquestra* CCMP 448	1	8	5	13	5	4	0	0	3
Dinoflagellata	*Karenia brevis* CCMP2229	1	14	8	10	8	7	0	1	4
Dinoflagellata	*Karenia brevis* SP1	1	14	13	16	6	8	0	1	4
Dinoflagellata	*Karenia brevis* SP3	1	12	9	13	8	10	0	1	4
Dinoflagellata	*Karenia brevis* Wilson	1	14	7	14	9	8	0	2	5
Dinoflagellata	*Karlodinium micrum* CCMP2283	2	9	7	46	13	31	2	0	5
Dinoflagellata	*Kryptoperidinium foliaceum* CCMP1326	4	14	11	64	16	10	1	0	7
Dinoflagellata	*Lingulodinium polyedra* CCMP1738	1	17	8	19	11	11	1	0	3
Dinoflagellata	*Noctiluca scintillans* Unknown	1	7	3	9	1	6	0	1	1
Dinoflagellata	*Oxyrrhis marina*	1	2	5	9	7	3	0	1	2
Dinoflagellata	*Oxyrrhis marina* CCMP1795	0	0	0	0	3	0	0	0	0
Dinoflagellata	*Oxyrrhis marina* LB1974	1	2	4	10	4	2	0	0	2
Dinoflagellata	*Pelagodinium beii* RCC1491	1	8	2	12	11	4	0	0	4
Dinoflagellata	*Peridinium aciculiferum* PAER_2	1	7	5	11	6	5	0	0	3
Dinoflagellata	*Polarella glacialis* CCMP 1383	1	28	5	23	5	5	0	0	8

Continued on next page

Supplementary Table 2 – *Continued from previous page*

clade	species	TOP1	TOP2	TOP3	MCM	PCNA	RPA1	RPA2	RPA3	RFC1
Dinoflagellata	*Prorocentrum minimum* CCMP1329	1	15	6	29	13	6	0	0	3
Dinoflagellata	*Prorocentrum minimum* CCMP2233	1	14	4	29	12	5	0	0	3
Dinoflagellata	*Protoceratium reticulatum* CCCM 535 CCMP 1889	2	20	9	18	11	10	0	0	2
Dinoflagellata	*Pyrodinium bahamense* pbaha01	1	21	8	29	19	11	0	0	3
Dinoflagellata	*Scrippsiella hangoei* like SHHI_4	1	8	6	22	6	16	0	2	2
Dinoflagellata	*Scrippsiella hangoei* SHTV5	1	8	11	14	3	5	0	0	2
Dinoflagellata	*Scrippsiella trochoidea* CCMP3099	1	27	10	38	12	8	1	1	3
Dinoflagellata	*Symbiodinium kawagutii* CCMP2468	0	0	0	0	2	0	0	0	0
Dinoflagellata	*Symbiodinium* sp. C1	1	9	4	9	6	4	0	0	3
Dinoflagellata	*Symbiodinium* sp. C15	1	7	2	12	3	4	1	0	3
Dinoflagellata	*Symbiodinium* sp. CCMP2430	1	7	2	10	7	4	0	0	3
Dinoflagellata	*Symbiodinium* sp. Mp	1	7	3	13	6	3	0	0	3
Dinoflagellata	*Togula jolla* CCCM 725	1	17	3	21	3	6	0	0	4
Discosea	*Mayorella* sp. BSH 02190019	1	3	2	5	1	1	0	1	1
Discosea	*Neoparamoeba aestuarina* SoJaBio B1 5 56 2	3	3	3	12	3	3	0	1	1
Discosea	*Paramoeba atlantica* 621 1 CCAP 1560 9	1	3	2	8	3	2	0	1	1
Discosea	*Pessonella* sp. PRA 29	1	1	3	0	1	5	0	2	3
Discosea	*Stygamoeba regulata* BSH 02190019	3	8	2	7	2	4	0	0	2
Discosea	*Trichosphaerium* sp. Am I 7 wt	2	0	0	1	2	3	0	0	2
Eugelnophyta	*Eutreptiella gymnastica* like CCMP1594	1	1	1	5	2	1	0	1	1
Foraminifera	*Ammonia* sp. Unknown	1	1	3	9	5	2	0	1	1
Foraminifera	*Elphidium margaritaceum* Unknown	1	1	2	8	3	1	1	0	1
Foraminifera	*Rosalina* sp. Unknown	1	0	0	9	5	0	2	0	1
Foraminifera	*Sorites* sp. Unknown	3	3	0	27	12	3	0	0	2
Fungi	*Debaryomyces hansenii* J26	1	0	0	4	0	0	0	0	1
Glaucophyte	*Gloeochaete witrockiana* SAG46_84	2	2	3	9	2	2	1	1	1
Haptophyte	*Calcidiscus leptoporus* RCC1130	1	3	0	7	1	1	1	0	1
Haptophyte	*Chrysochromulina brevifilum* UTEX LB 985	1	2	1	4	1	3	0	1	0
Haptophyte	*Chrysochromulina ericina* CCMP281	2	1	0	10	1	3	1	1	2
Haptophyte	*Chrysochromulina polylepis* CCMP1757	1	3	5	9	1	2	1	1	1
Haptophyte	*Chrysoculter rhomboideus* RCC1486	1	0	0	9	1	0	0	1	0
Haptophyte	*Coccolithus pelagicus* ssp *braarudi* PLY182g	1	3	0	7	1	2	1	1	0
Haptophyte	*Emiliania huxleyi* 374	1	2	1	9	1	1	0	0	0
Haptophyte	*Emiliania huxleyi* 379	1	1	1	0	0	2	0	0	0
Haptophyte	*Emiliania huxleyi* CCMP370	1	3	5	9	0	2	1	1	1
Haptophyte	*Emiliania huxleyi* PLYM219	1	3	4	10	0	2	1	1	1
Haptophyte	*Exanthemachrysis gayraliae* RCC1523	1	2	0	1	1	1	0	1	1
Haptophyte	*Gephyrocapsa oceanica* RCC1303	1	3	5	11	1	1	0	0	1
Haptophyte	*Imantonia* sp. RCC918	3	1	1	4	2	1	1	1	0
Haptophyte	*Isochrysis galbana* CCMP1323	2	5	6	13	2	3	1	0	2
Haptophyte	*Isochrysis* sp. CCMP1244	1	2	5	11	1	1	0	1	1
Haptophyte	*Isochrysis* sp. CCMP1324	1	2	0	12	1	2	1	0	1
Haptophyte	*Pavlova* sp. CCMP459	1	2	1	6	2	1	2	1	1
Haptophyte	*Phaeocystis antarctica* Caron Lab Isolate	3	7	2	12	1	3	2	0	2
Haptophyte	*Phaeocystis* sp. CCMP2710	1	0	1	2	1	1	1	1	1
Haptophyte	*Pleurochrysis carterae* CCMP645	3	2	1	7	1	2	1	1	1
Haptophyte	*Prymnesium parvum* Texoma1	1	6	4	1	1	2	1	1	1
Haptophyte	*Scyphosphaera apsteinii* RCC1455	1	3	1	7	1	2	1	0	1
Heterolobosea	*Percolomonas cosmopolitus* AE 1 ATCC 50343	1	4	2	9	2	2	0	0	1
Heterolobosea	*Percolomonas cosmopolitus* WS	1	3	1	12	1	2	0	0	3
Khakista	*Corethron pennatum* L29A3	2	5	5	16	1	1	1	0	1
Khakista	*Detonula confervacea* CCMP 353	1	3	2	9	1	1	2	1	1
Kinetoplastida	*Neobodo designis* CCAP 1951 1	1	1	4	8	1	1	0	0	1
Labyrinthulida	*Aplanochytrium* sp. PBS07	1	2	1	3	1	1	1	2	1
Labyrinthulida	*Aplanochytrium stocchinoi* GSBS06	1	2	0	7	1	1	1	1	1
Pelagophyte	*Aureococcus anophagefferens* CCMP1850	6	2	3	45	1	2	0	0	1
Pelagophyte	*Aureoumbra lagunensis* CCMP1510	1	2	2	9	1	2	1	0	1
Pelagophyte	*Chrysocystis fragilis* CCMP3189	2	0	2	6	1	1	1	0	1

Continued on next page

Supplementary Table 2 – *Continued from previous page*

clade	species	TOP1	TOP2	TOP3	MCM	PCNA	RPA1	RPA2	RPA3	RFC1
Pelagophyte	*Chrysoreinhardia* sp. CCMP2950	1	2	1	5	0	1	0	0	1
Pelagophyte	*Chrysoreinhardia* sp. CCMP3193	1	3	2	10	1	2	1	0	1
Pelagophyte	*Pelagomonas calceolata* CCMP1756	1	2	1	9	1	1	2	0	1
Pelagophyte	*Sarcinochrysis* sp. CCMP770	0	0	0	2	1	1	1	1	0
Perkinsid	*Perkinsus chesapeaki* ATCC_PRA_65	2	0	0	0	0	0	0	0	0
Perkinsid	*Perkinsus marinus* ATCC50439	1	0	0	1	2	0	0	0	0
Pinguiophyte	*Phaeomonas parva* CCMP2877	1	3	1	5	3	1	0	1	0
Pinguiophyte	*Pinguiococcus pyrenoidosus* CCMP2078	1	2	3	0	1	1	0	1	0
Raphidophyte	*Chattonella subsalsa* CCMP2191	1	3	0	5	1	1	1	0	1
Raphidophyte	*Fibrocapsa japonica* CCMP1661	0	1	1	5	1	1	0	1	0
Raphidophyte	*Heterosigma akashiwo* CCMP2393	1	4	2	11	2	1	0	1	1
Raphidophyte	*Heterosigma akashiwo* CCMP3107	1	7	2	0	1	1	0	0	0
Raphidophyte	*Heterosigma akashiwo* CCMP452	0	1	0	4	1	1	0	0	0
Raphidophyte	*Heterosigma akashiwo* NB	1	6	1	8	1	1	0	1	1
Rhodophyte	*Compsopogon coeruleus* SAG 36.94	1	3	2	11	1	1	0	0	1
Rhodophyte	*Erythrolobus australicus* CCMP3124	1	2	3	0	1	1	0	1	1
Rhodophyte	*Erythrolobus madagascarensis* CCMP3276	1	1	1	3	1	2	0	1	0
Rhodophyte	*Madagascaria erythrocladiodes* CCMP3234	3	4	5	12	1	2	0	1	2
Rhodophyte	*Porphyridium aerugineum* SAG 1380 2	2	1	2	5	1	2	1	0	1
Rhodophyte	*Rhodella maculata* CCMP736	1	3	3	12	1	1	0	0	1
Rhodophyte	*Rhodosorus marinus* CCMP 769	1	8	6	17	0	3	0	0	2
Rhodophyte	*Timspurckia oligopyrenoides* CCMP3278	1	2	4	6	1	2	1	1	1
Silicoflagellates	*Dictyocha speculum* CCMP1381	1	4	2	9	1	2	1	1	1
Silicoflagellates	*Pseudopedinella elastica* CCMP716	1	5	6	9	1	1	1	1	1
Silicoflagellates	*Pteridomonas danica* PT	1	1	1	2	1	1	1	1	0
Silicoflagellates	*Rhizochromulina marina* cf CCMP1243	1	5	2	8	2	2	1	1	1
Synchromophyceae	*Synchroma pusillum* CCMP3072	1	0	1	3	3	1	0	1	1
Syndinian	*Amoebophrya* sp. Ameob2	2	8	1	13	0	1	0	0	0
Thraustochytrid	*Aurantiochytrium limacinum* ATCCMYA1381	1	3	2	9	1	1	0	1	1
Thraustochytrid	*Schizochytrium aggregatum* ATCC28209	1	1	1	4	1	1	0	0	1
Thraustochytrid	*Thraustochytrium* sp. LLF1b	1	2	1	9	1	1	0	1	1
Tubulinid	*Filamoeba nolandi* NC AS 23 1	2	4	1	13	0	3	1	0	1
Tubulinid	*Sexangularia* sp. ATCC50979	0	6	7	14	2	2	1	0	3
Vanellinid	*Vannella robusta* DIVA3 518 3 11 1 6	1	2	3	6	1	2	1	1	1
Vanellinid	*Vannella* sp. DIVA3 517 6 12	6	6	9	13	1	1	0	1	1
Xantophyte	*Vaucheria litorea* CCMP2940	1	2	0	6	1	1	0	1	1

Supplementary Figures

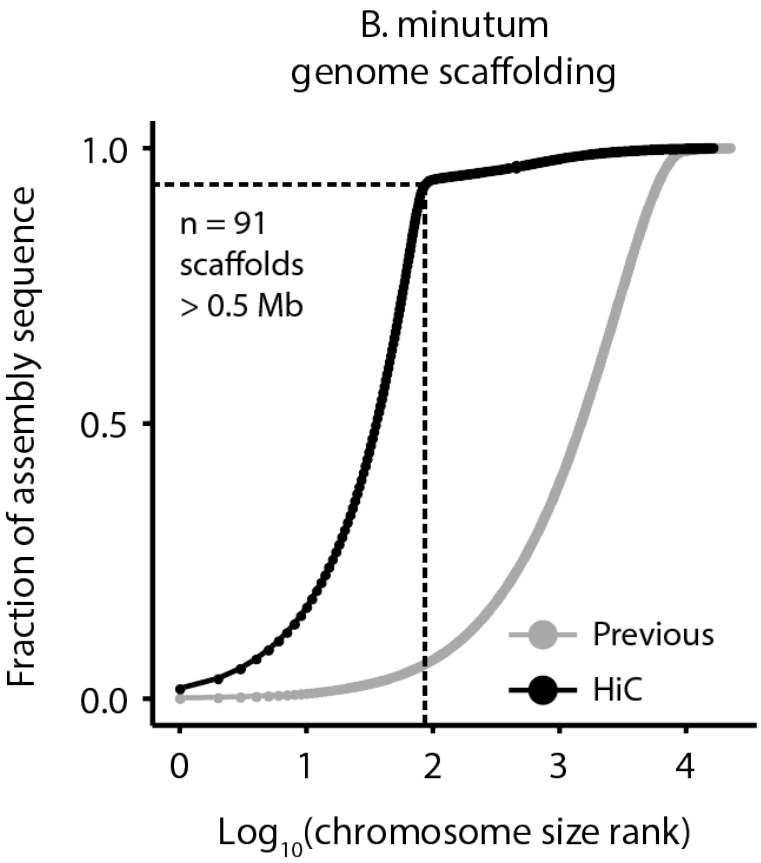

Supplementary Figure 1: Cumulative distribution of scaffolds and pseudochromosome sizes before and after Hi-C scaffolding of the draft *Breviolum/Symbiodinium minutum* assembly[6]. 3D DNA[18] scaffolding of the assembly results in 91 major pseudochromosomes ≥500kb encompassing ∼94% of the assembled sequence.

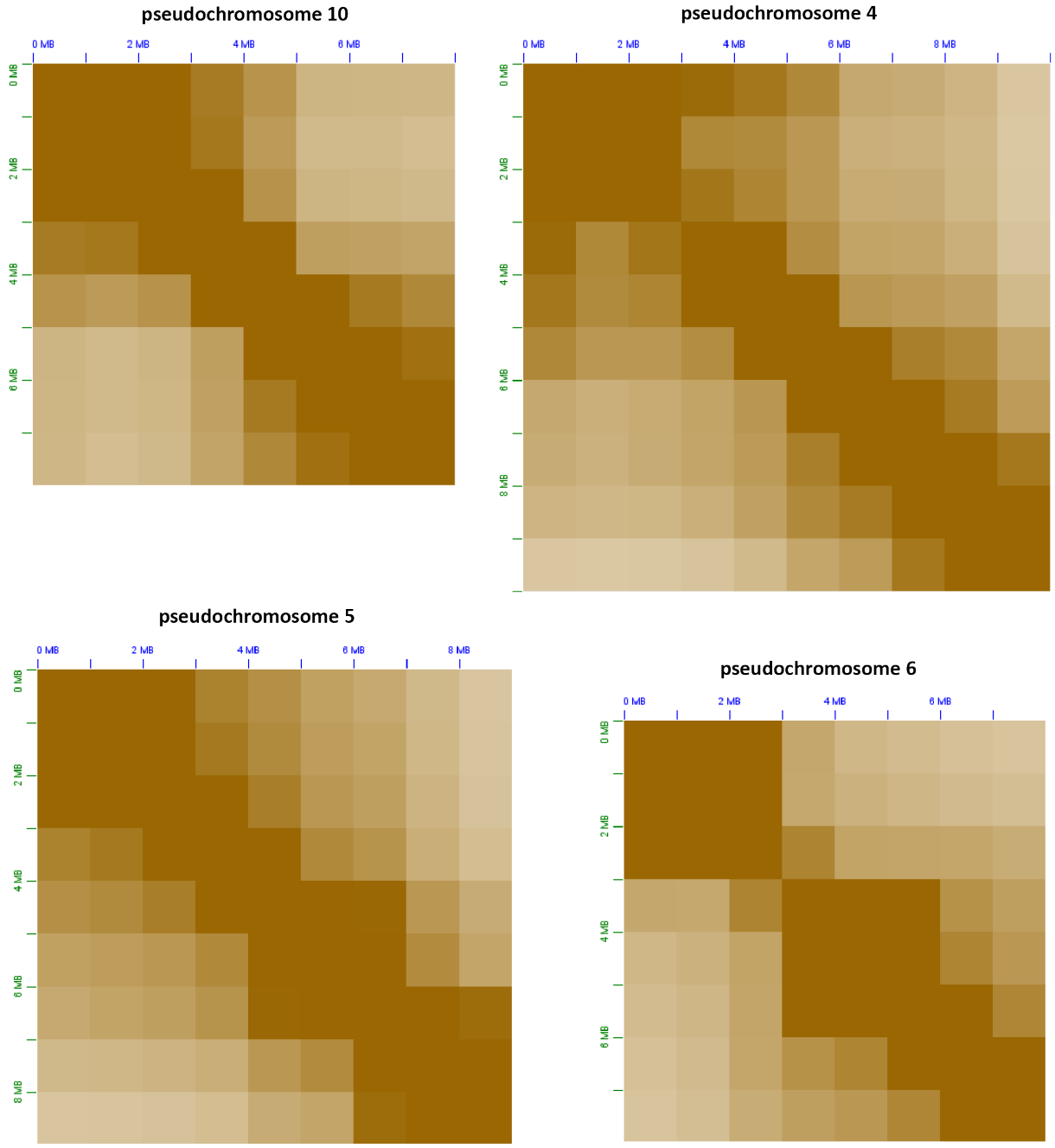

Supplementary Figure 2: Broad-level bipartite to tripartite topological structure of dinoflagellate chromosomes. Shown are 1Mbp-resolution KR-normalized[24] Hi-C matrices for four of the *B. minutum* pseudochromosomes.

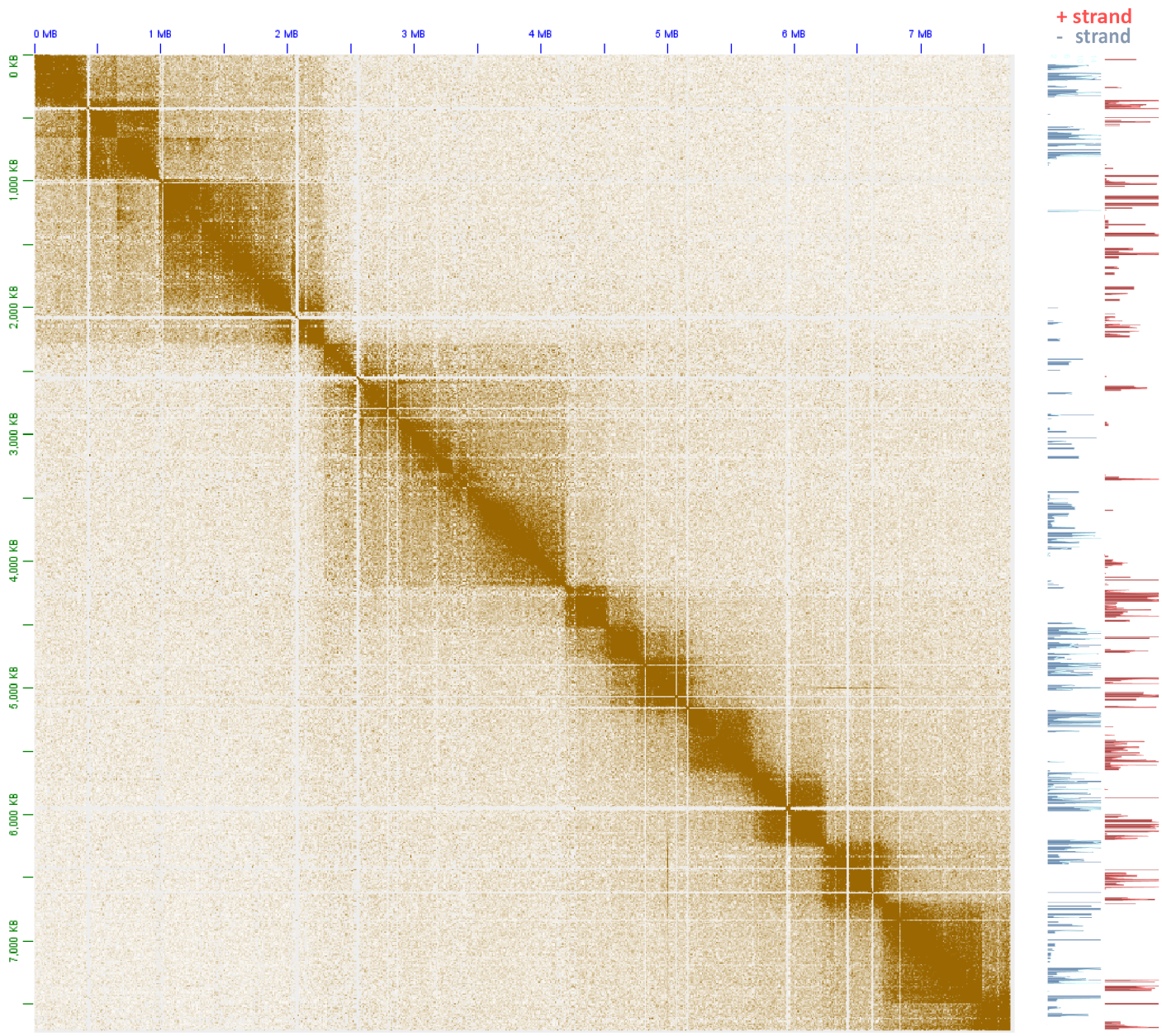

Supplementary Figure 3: The topological domain organization of dinoflagellate chromosomes is related to polycistronic gene array orientation. Shown is the 5kb-resolution KR-normalized Hi-C map together with strand-specific RNA expression levels for pseudochromosome 17.

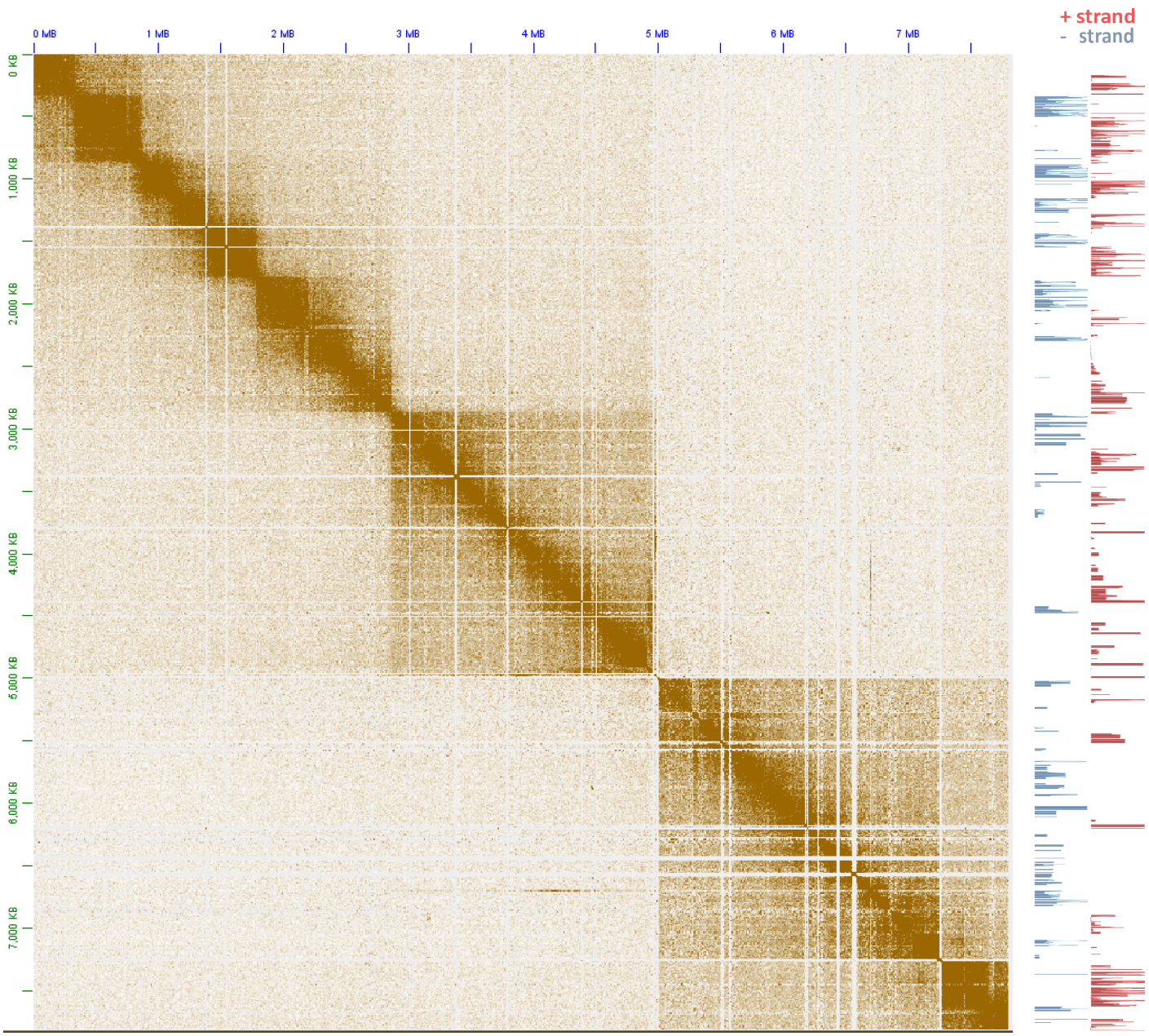

Supplementary Figure 4: The topological domain organization of dinoflagellate chromosomes is related to polycistronic gene array orientation. Shown is the 5kb-resolution KR-normalized Hi-C map together with strand-specific RNA expression levels for pseudochromosome 18.

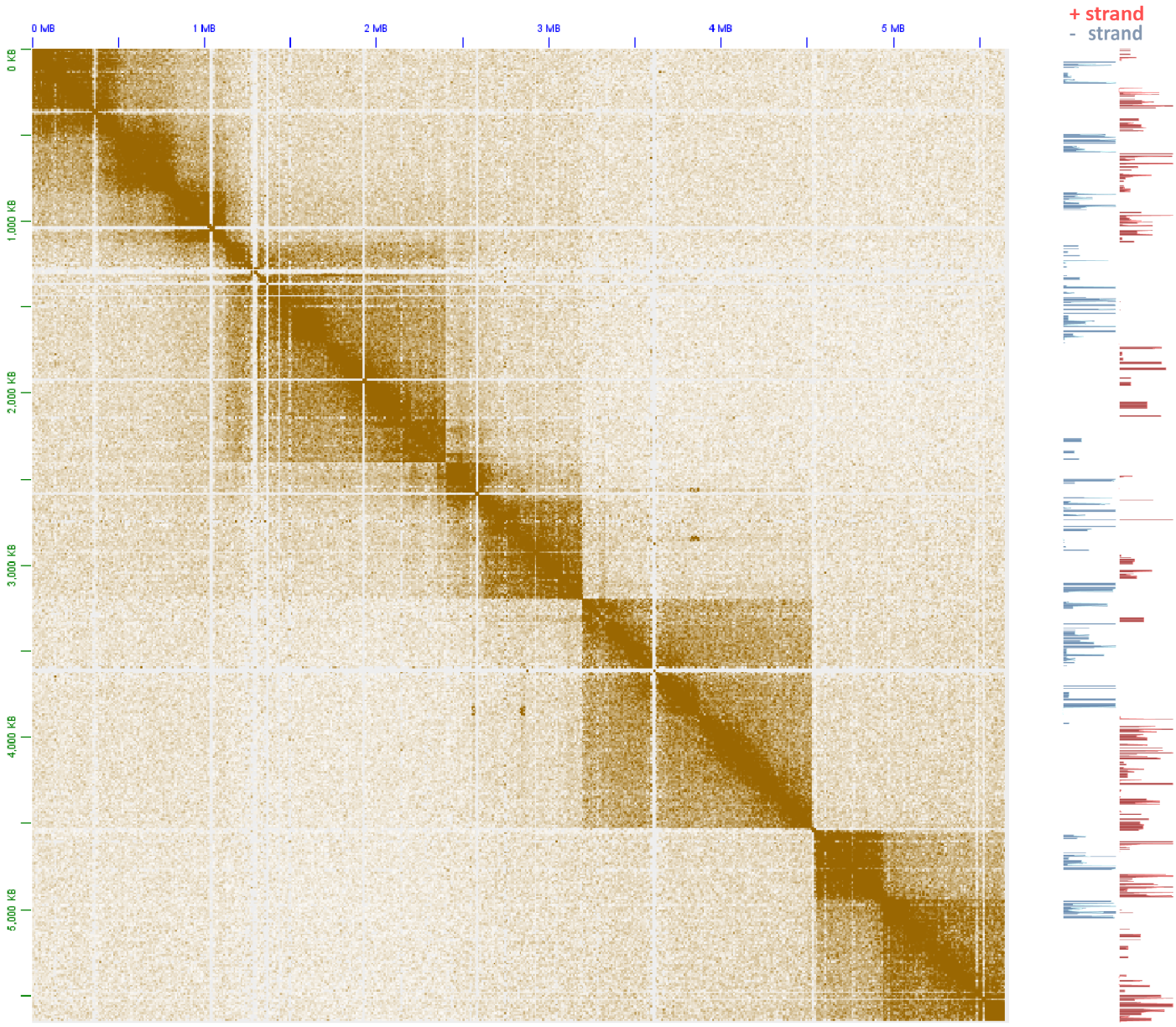

Supplementary Figure 5: The topological domain organization of dinoflagellate chromosomes is related to polycistronic gene array orientation. Shown is the 5kb-resolution KR-normalized Hi-C map together with strand-specific RNA expression levels for pseudochromosome 21.

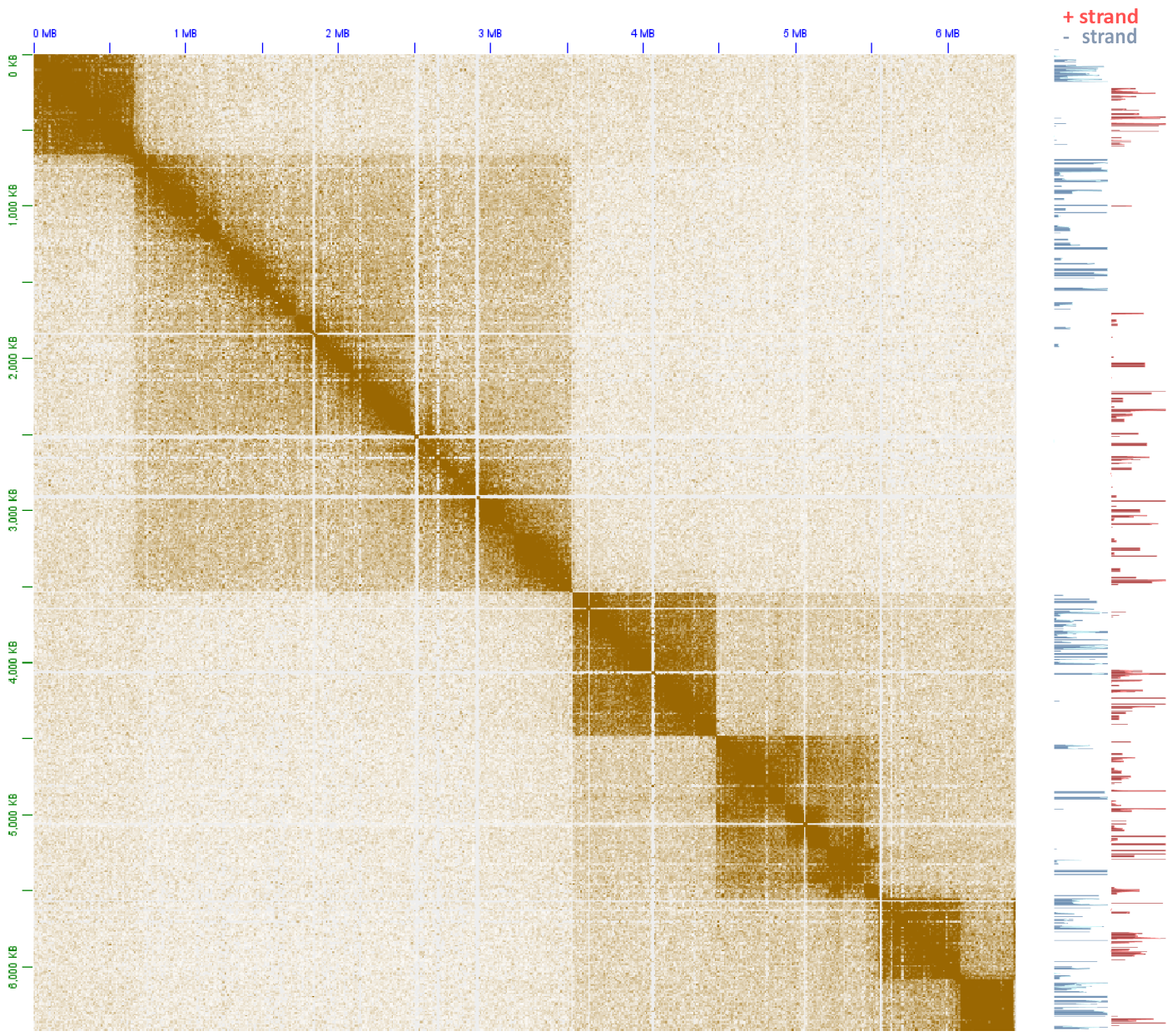

Supplementary Figure 6: The topological domain organization of dinoflagellate chromosomes is related to polycistronic gene array orientation. Shown is the 5kb-resolution KR-normalized Hi-C map together with strand-specific RNA expression levels for pseudochromosome 26.

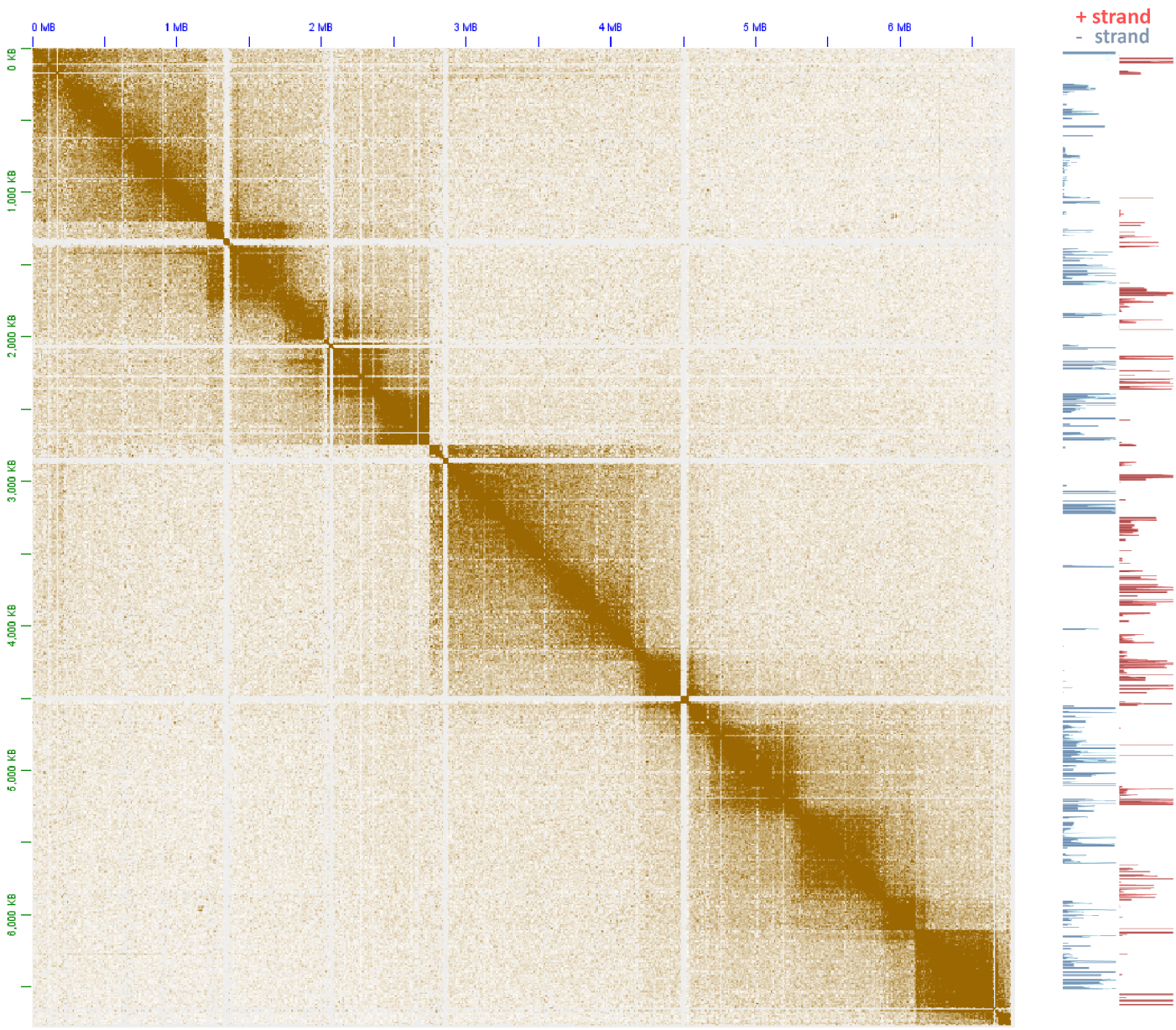

Supplementary Figure 7: The topological domain organization of dinoflagellate chromosomes is related to polycistronic gene array orientation. Shown is the 5kb-resolution KR-normalized Hi-C map together with strand-specific RNA expression levels for pseudochromosome 32.

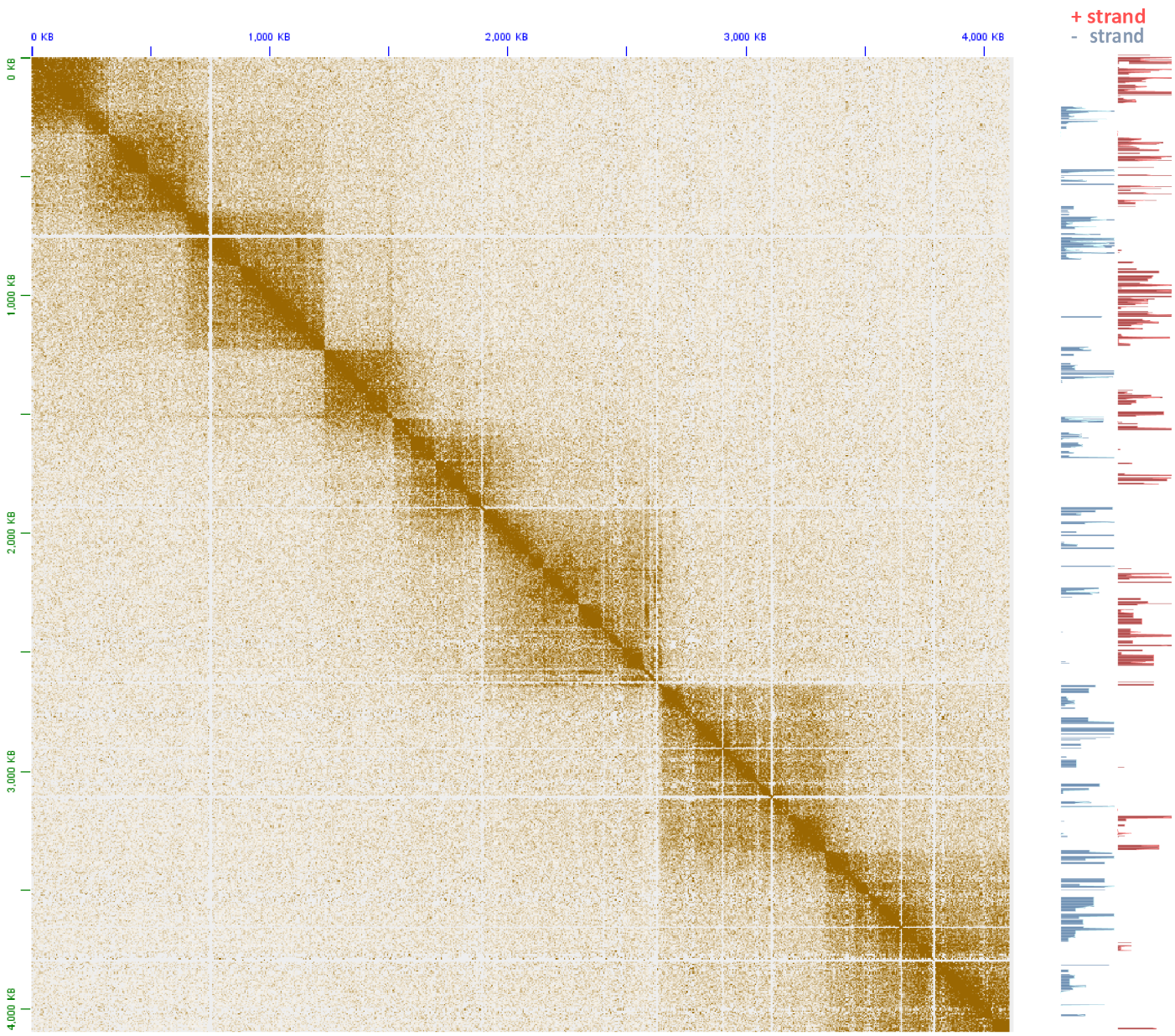

Supplementary Figure 8: The topological domain organization of dinoflagellate chromosomes is related to polycistronic gene array orientation. Shown is the 5kb-resolution KR-normalized Hi-C map together with strand-specific RNA expression levels for pseudochromosome 36.

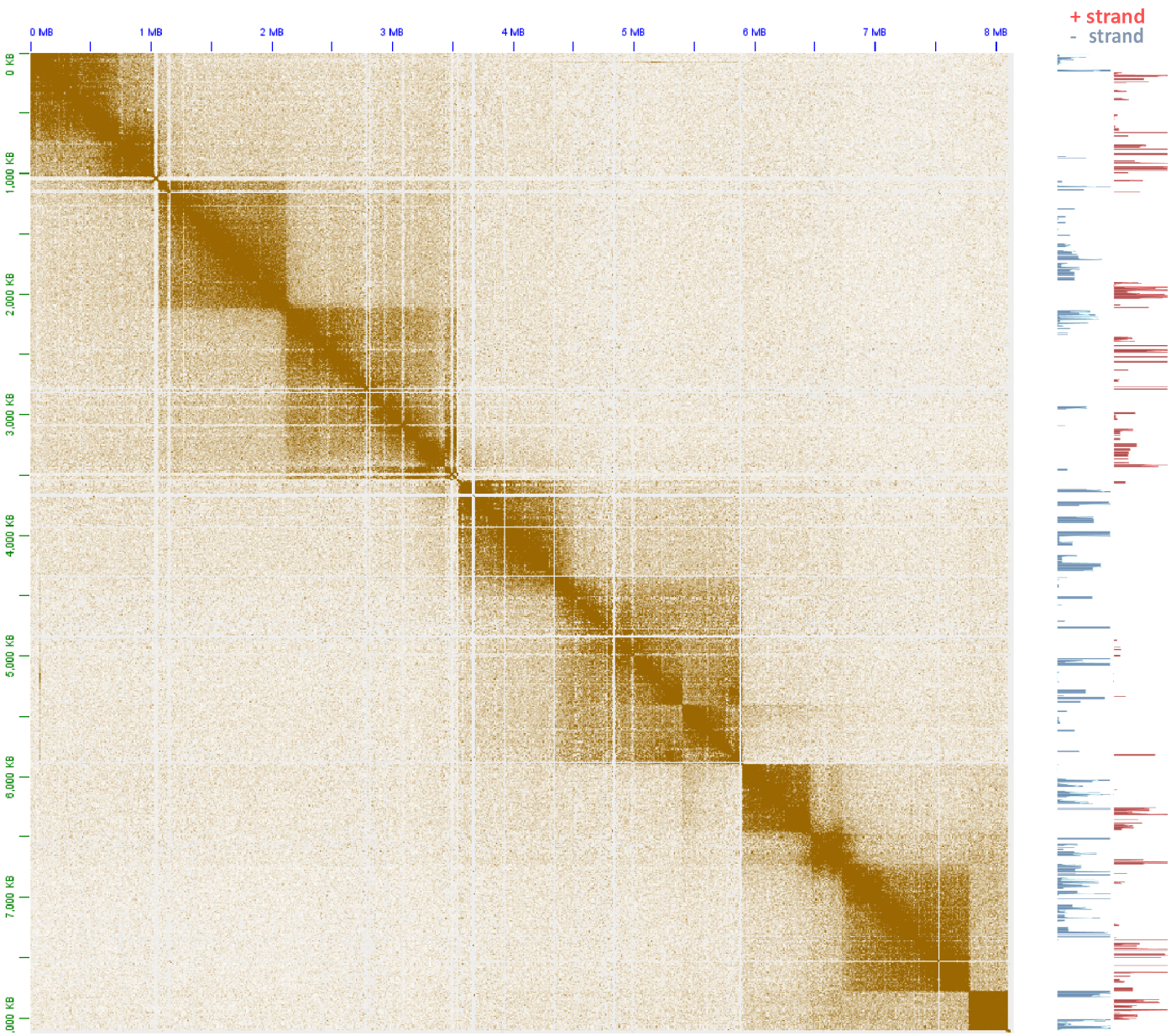

Supplementary Figure 9: The topological domain organization of dinoflagellate chromosomes is related to polycistronic gene array orientation. Shown is the 5kb-resolution KR-normalized Hi-C map together with strand-specific RNA expression levels for pseudochromosome 71.

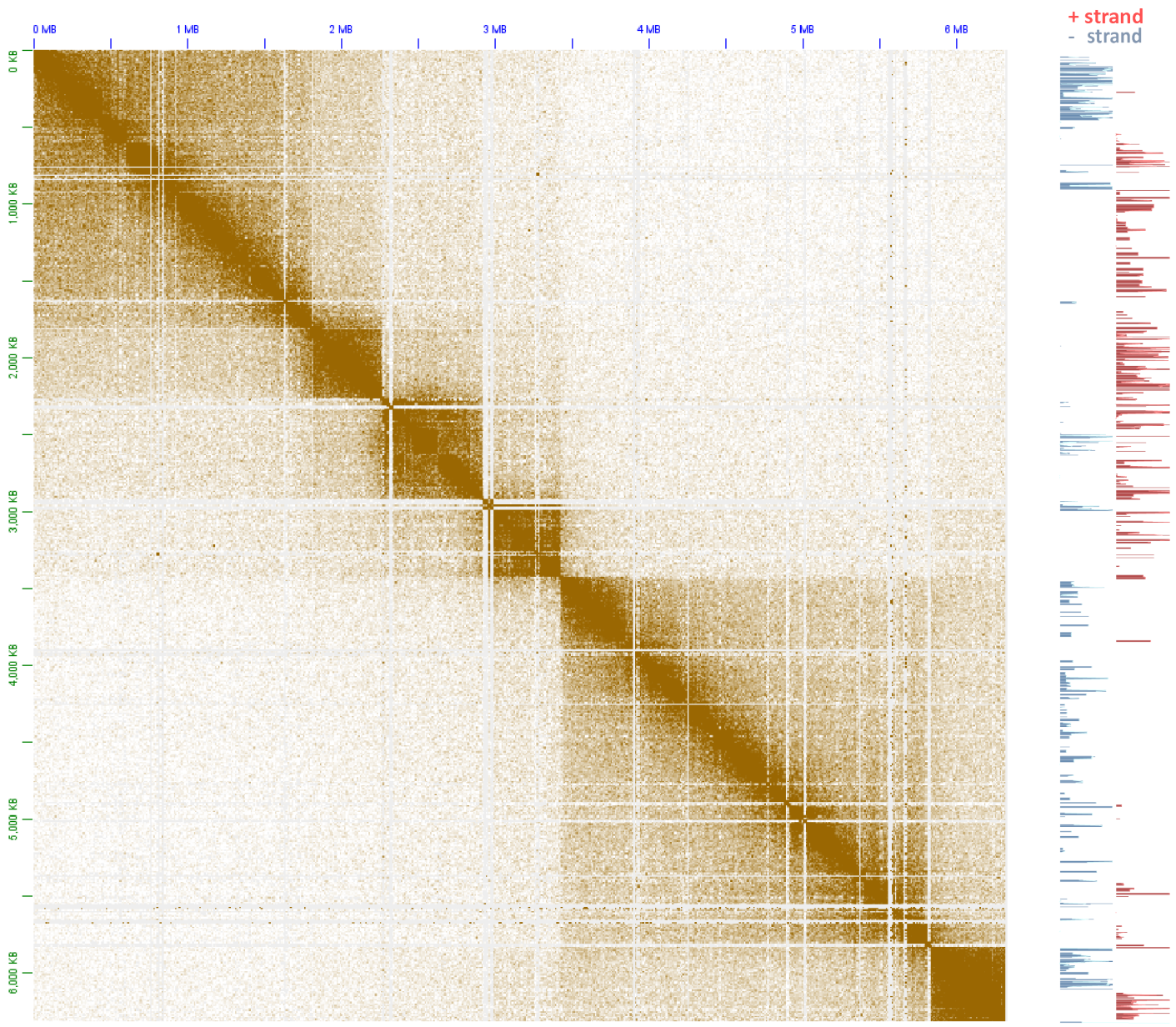

Supplementary Figure 10: The topological domain organization of dinoflagellate chromosomes is related to polycistronic gene array orientation. Shown is the 5kb-resolution KR-normalized Hi-C map together with strand-specific RNA expression levels for pseudochromosome 77.

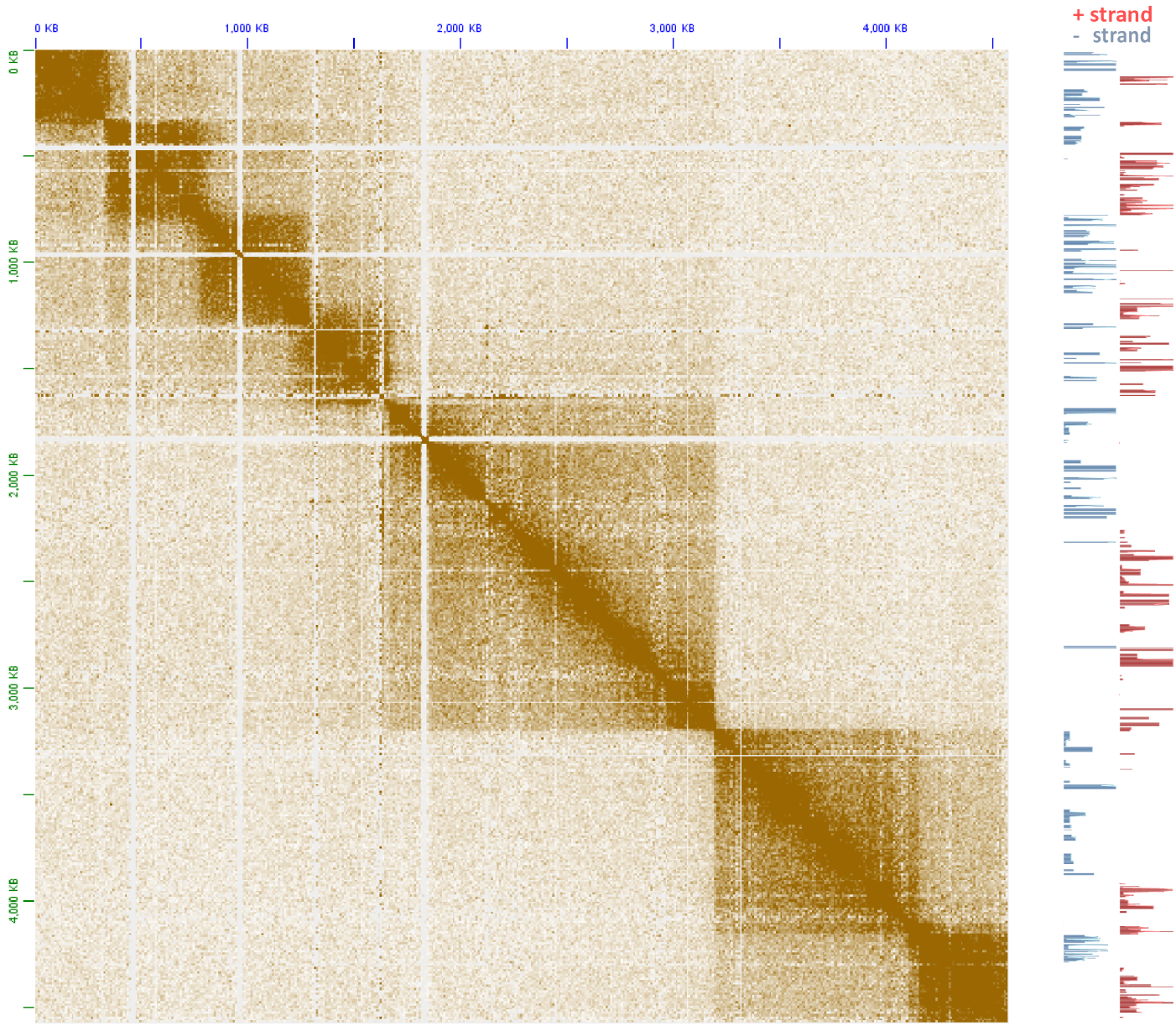

Supplementary Figure 11: The topological domain organization of dinoflagellate chromosomes is related to polycistronic gene array orientation. Shown is the 5kb-resolution KR-normalized Hi-C map together with strand-specific RNA expression levels for pseudochromosome 78.

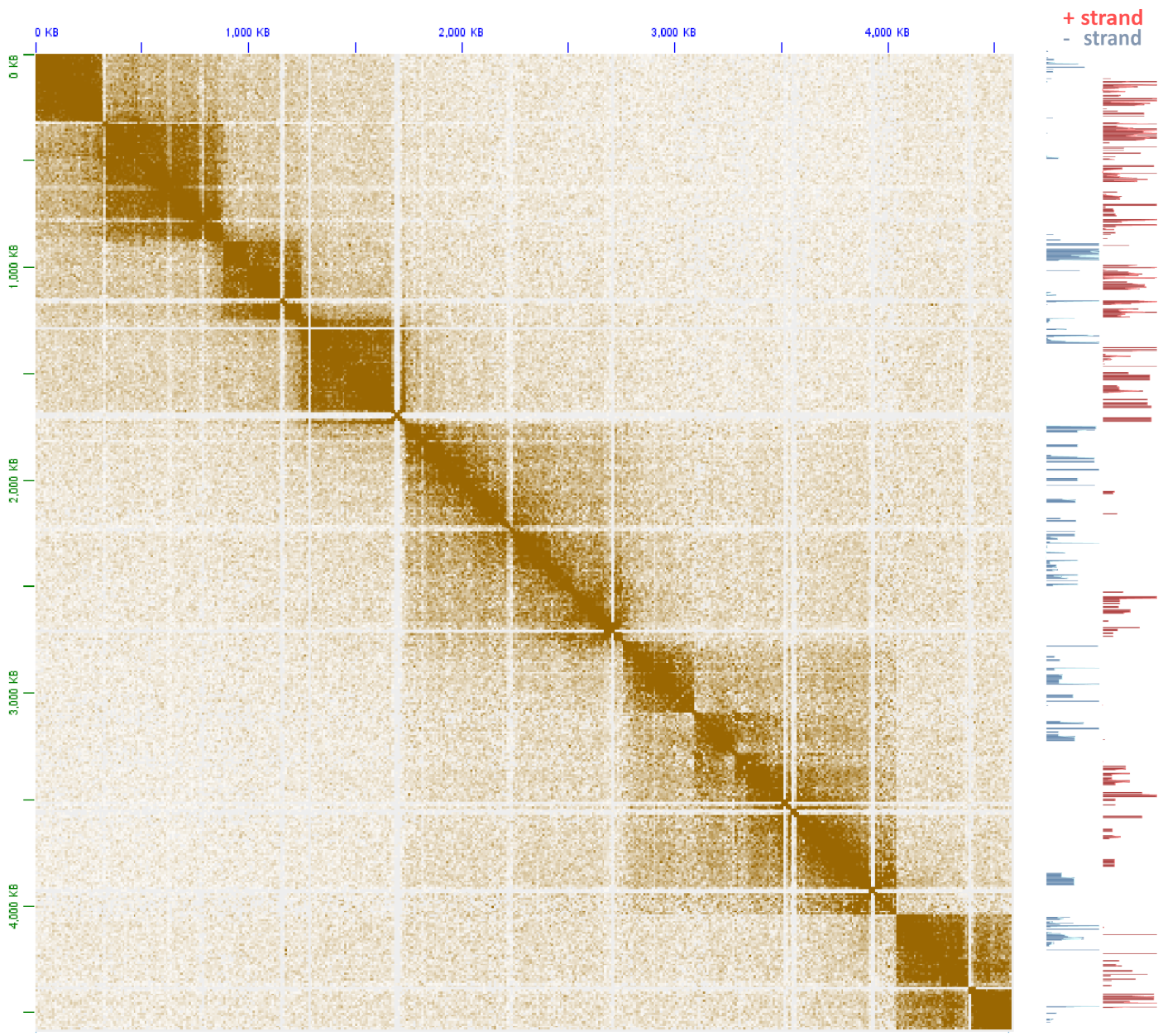

Supplementary Figure 12: The topological domain organization of dinoflagellate chromosomes is related to polycistronic gene array orientation. Shown is the 5kb-resolution KR-normalized Hi-C map together with strand-specific RNA expression levels for pseudochromosome 88.

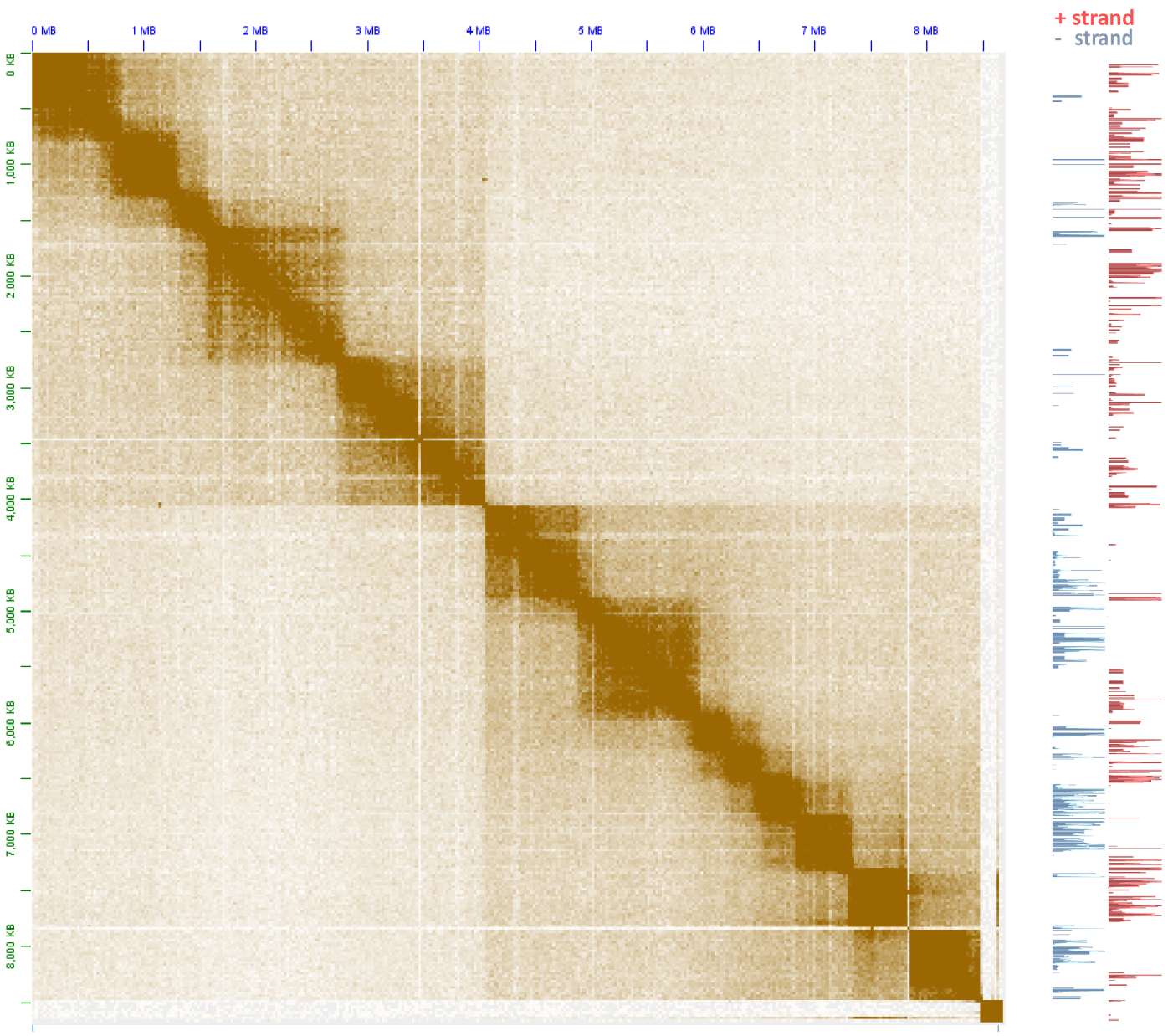

Supplementary Figure 13: The topological domain organization of dinoflagellate chromosomes is related to polycistronic gene array orientation. Shown is the 5kb-resolution KR-normalized Hi-C map together with strand-specific RNA expression levels for pseudochromosome 89.

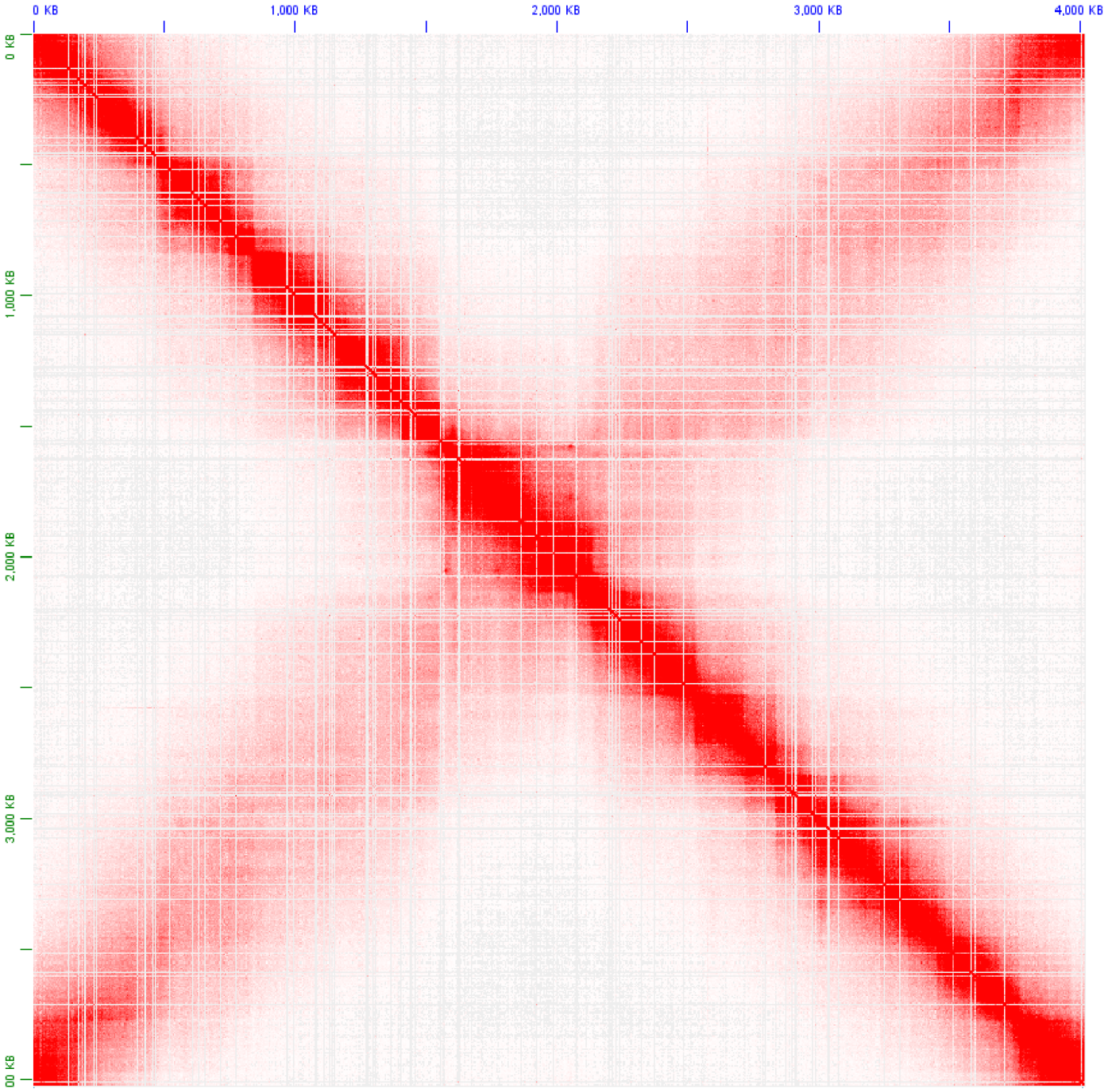

Supplementary Figure 14: Topological structure of the *Caulobacter crescentus* CB15 genome. Shown is the KR-normalized 5-kb resolution maps for the whole *Caulobacter* chromosome (GEO accession GSM1120448).

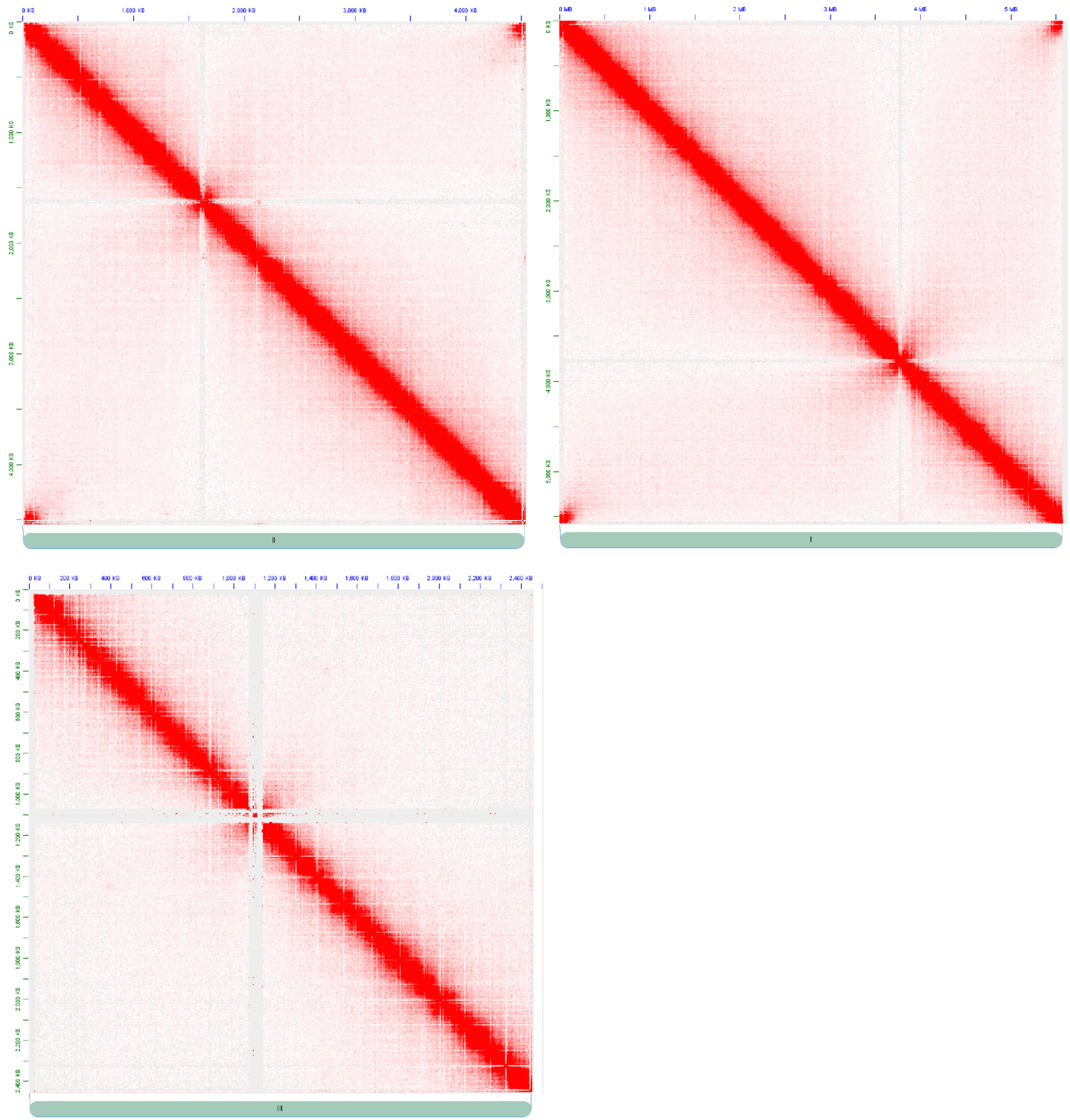

Supplementary Figure 15: Topological structure of the *Schizosaccharomyces pombe* genome. Shown are the KR-normalized 5-kb resolution maps for all three *S. pombe* chromosome (GEO accession GSM1379427).

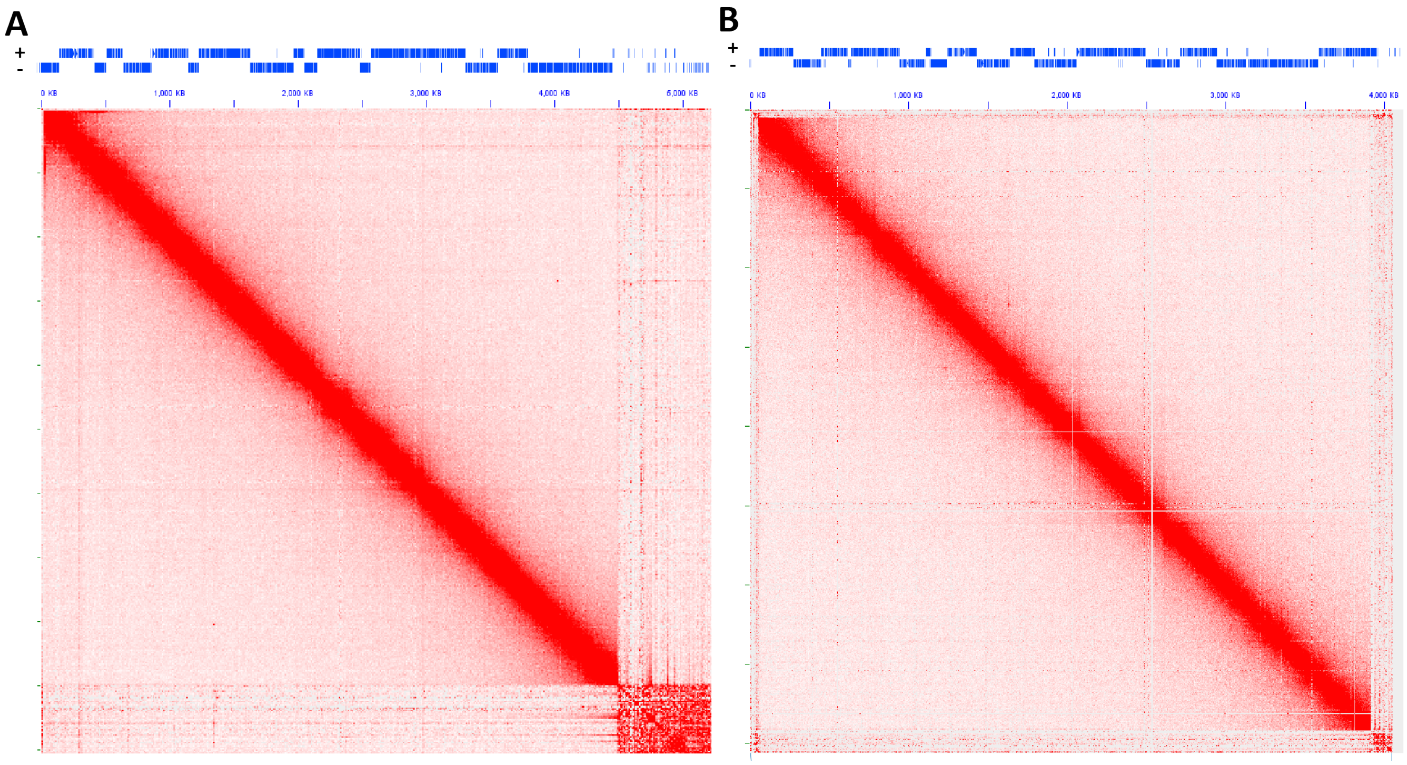

Supplementary Figure 16: No topological domains associated with gene arrays are observed in the kinetoplastid *Trypanosoma brucei*. Shown are KR-normalized 10-kb resolution maps for chr11 (A) and chr10 (B) for GEO accession GSM3346690.

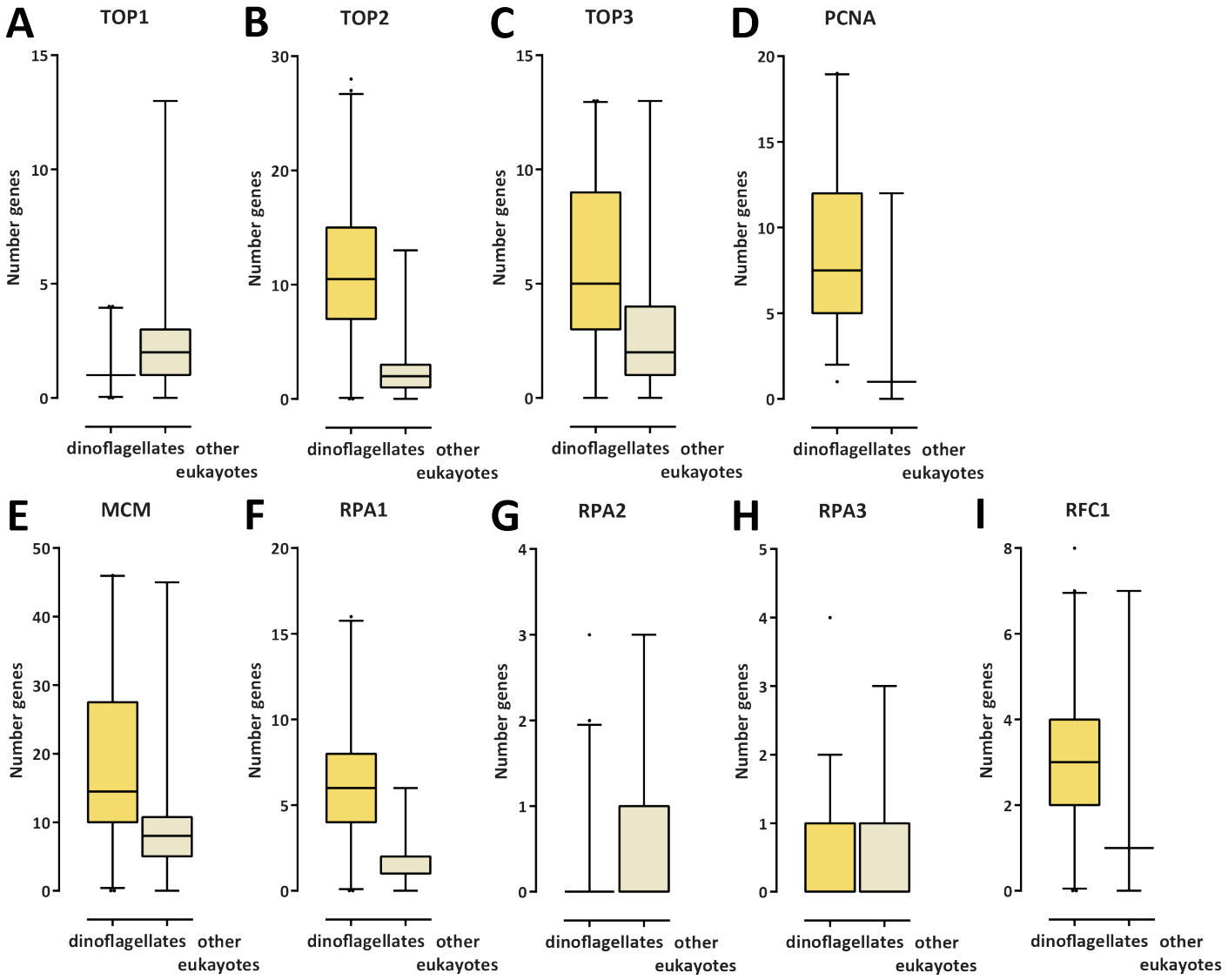

Supplementary Figure 17: Expansion of the Type II and II topoisomerase gene repertoire as well as of certain other replication-related proteins in dinoflagellates. Shown are the number of genes annotated in MMETSP transcriptome assemblies of dinoflagellates and other eukaryotes. (A) Number of Type I topoisomerase genes; (B) Number of Type II topoisomerase genes; (C) Number of Type III topoisomerase genes; (D) Number of PCNA genes; (E) Number of MCM genes; (F) Number of RPA1 genes; (G) Number of RPA2 genes; (H) Number of RPA3 genes; (I) Number of RFC1 genes.

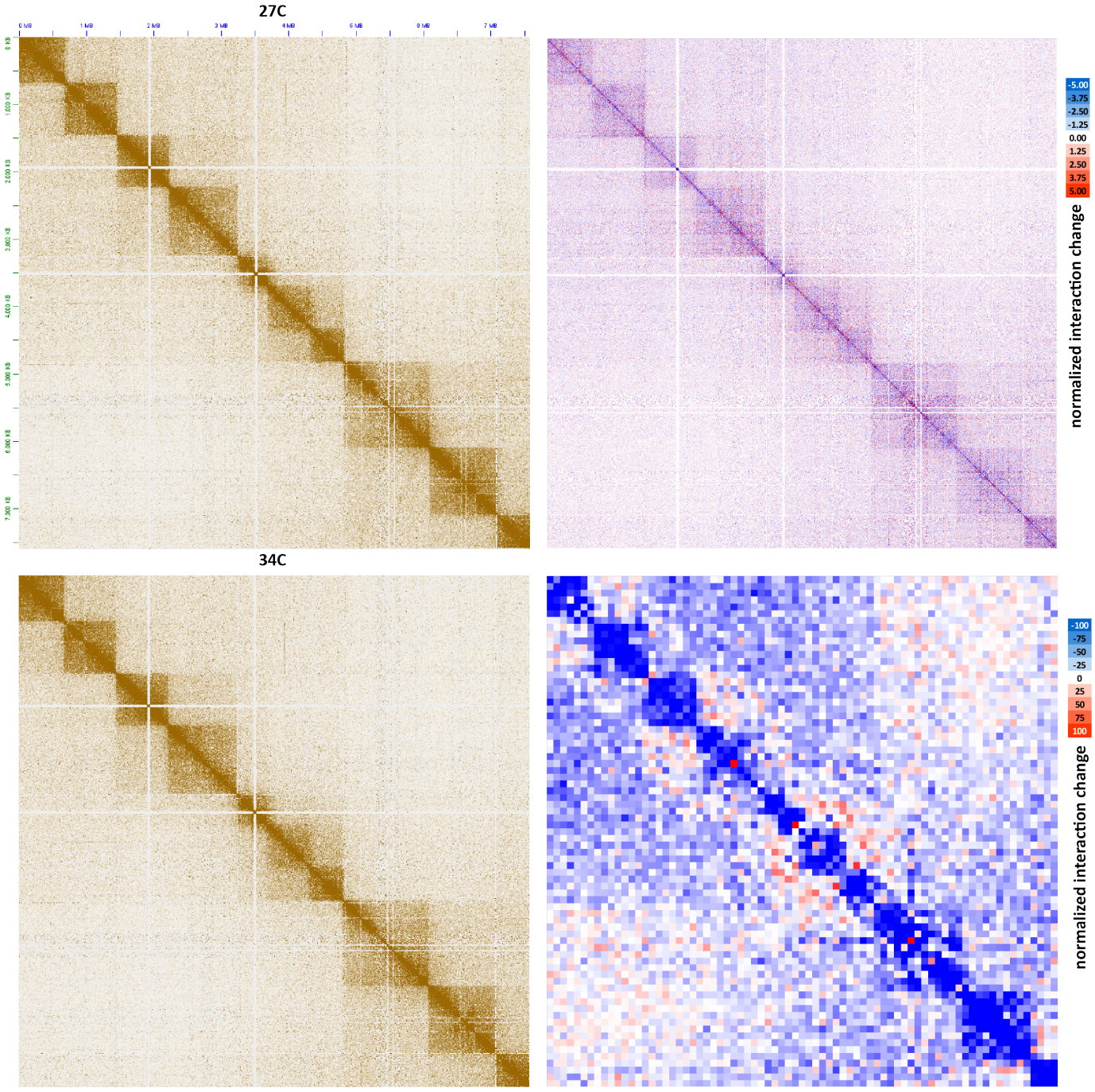

Supplementary Figure 18: Moderate decompaction of dinoTADs upon exposure to elevated temperatures. Shown is pseudochromosome 10 (KR-normalized) and the difference between the KR-normalized Hi-C maps generated from *B. minutum* grown at 34 °C and at 27 °C at 100-kb resolution (lower right) and 5-kb resolution (upper right).

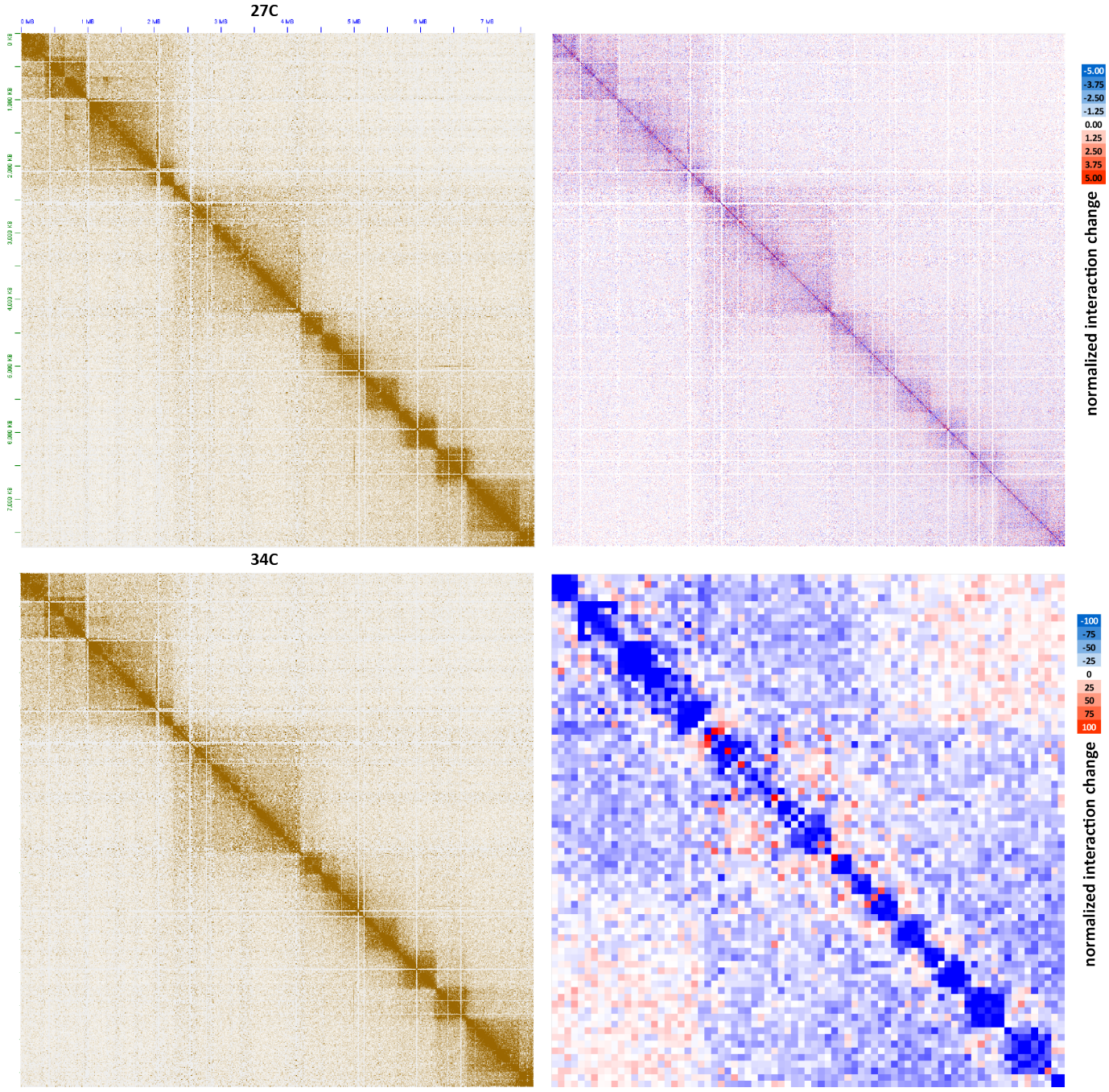

Supplementary Figure 19: Moderate decompaction of dinoTADs upon exposure to elevated temperatures. Shown is pseudochromosome 17 (KR-normalized) and the difference between the KR-normalized Hi-C maps generated from *B. minutum* grown at 34 °C and at 27 °C at 100-kb resolution (lower right) and 5-kb resolution (upper right).

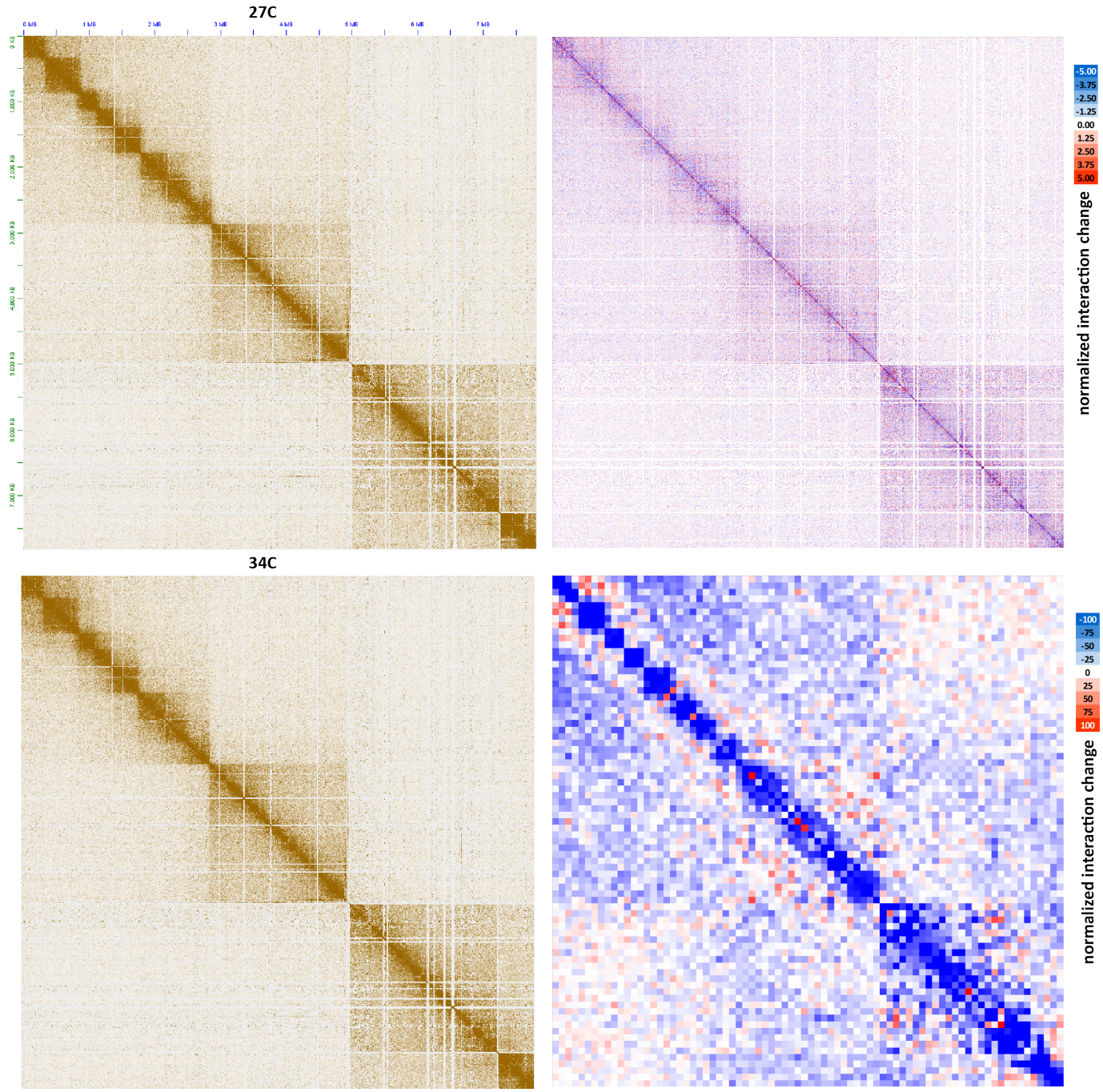

Supplementary Figure 20: Moderate decompaction of dinoTADs upon exposure to elevated temperatures. Shown is pseudochromosome 18 (KR-normalized) and the difference between the KR-normalized Hi-C maps generated from *B. minutum* grown at 34 °C and at 27 °C at 100-kb resolution (lower right) and 5-kb resolution (upper right).

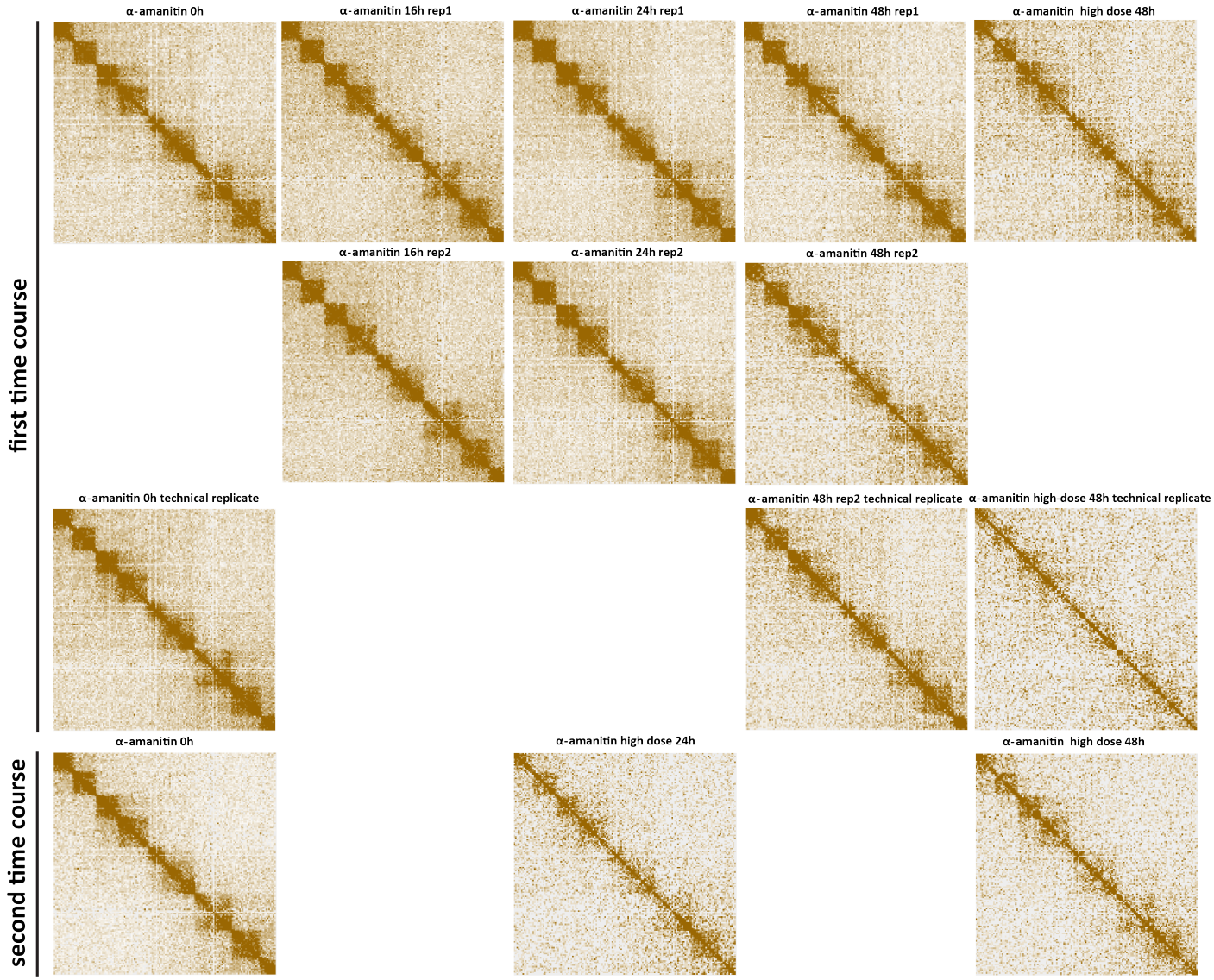

Supplementary Figure 21: Decompaction of dinoTADs upon transcriptional inhibition using α-amanitin. Shown is pseudochromosome 10. Two time courses were carried out following the outline presented in Figure 2B.

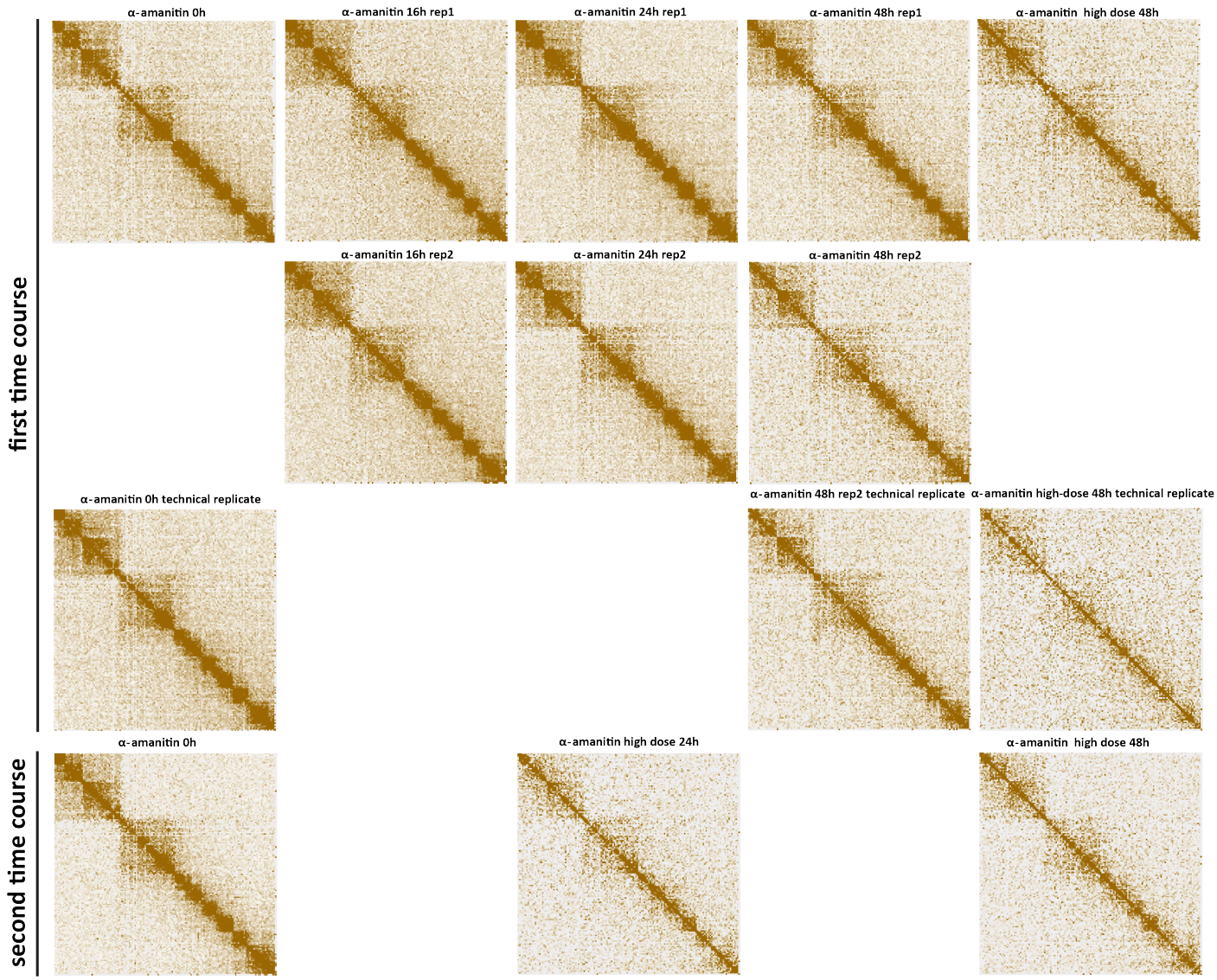

Supplementary Figure 22: Decompaction of dinoTADs upon transcriptional inhibition using α-amanitin. Shown is pseudochromosome 17. Two time courses were carried out following the outline presented in Figure 2B.

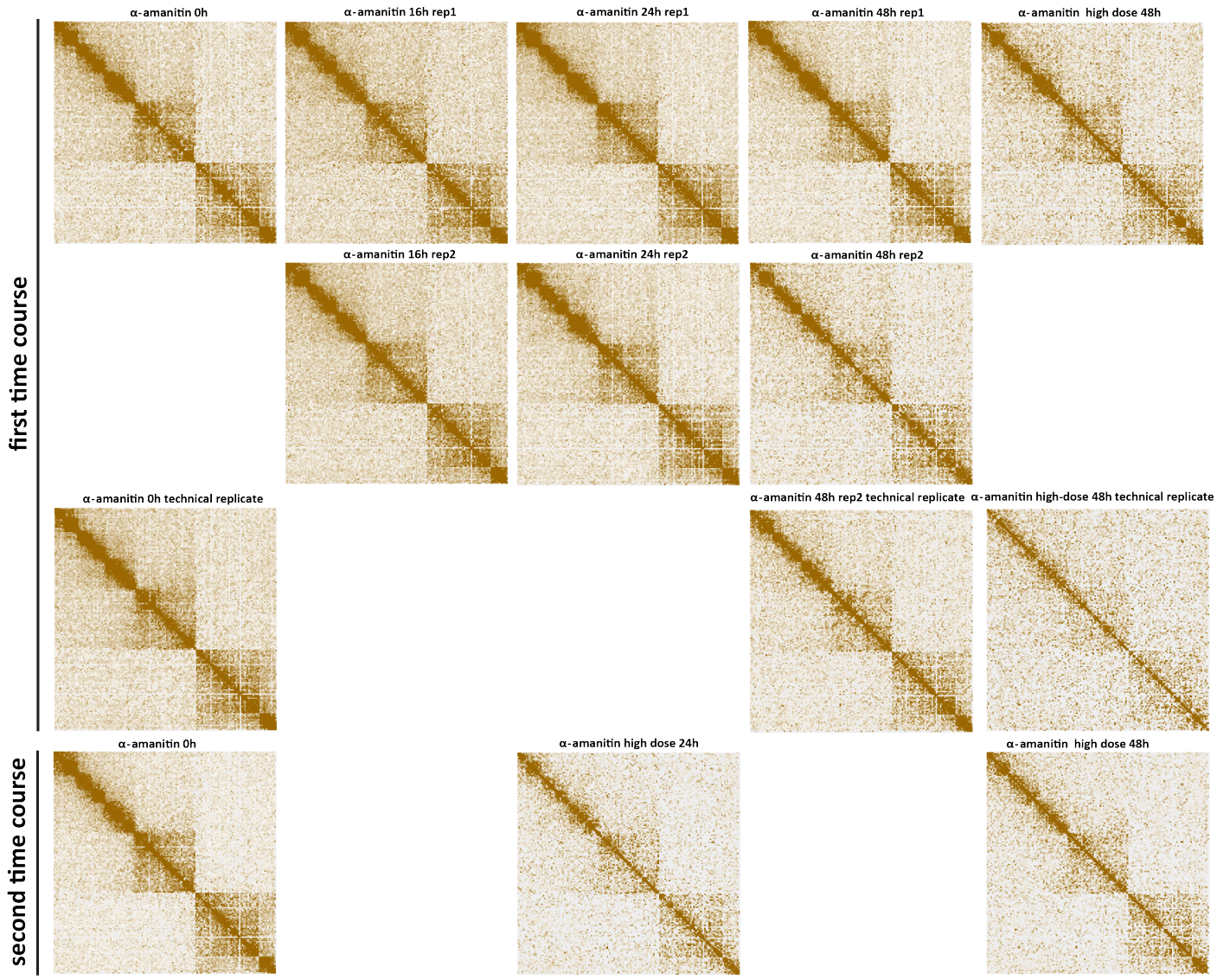

Supplementary Figure 23: Decompaction of dinoTADs upon transcriptional inhibition using α-amanitin. Shown is pseudochromosome 18. Two time courses were carried out following the outline presented in Figure 2B.

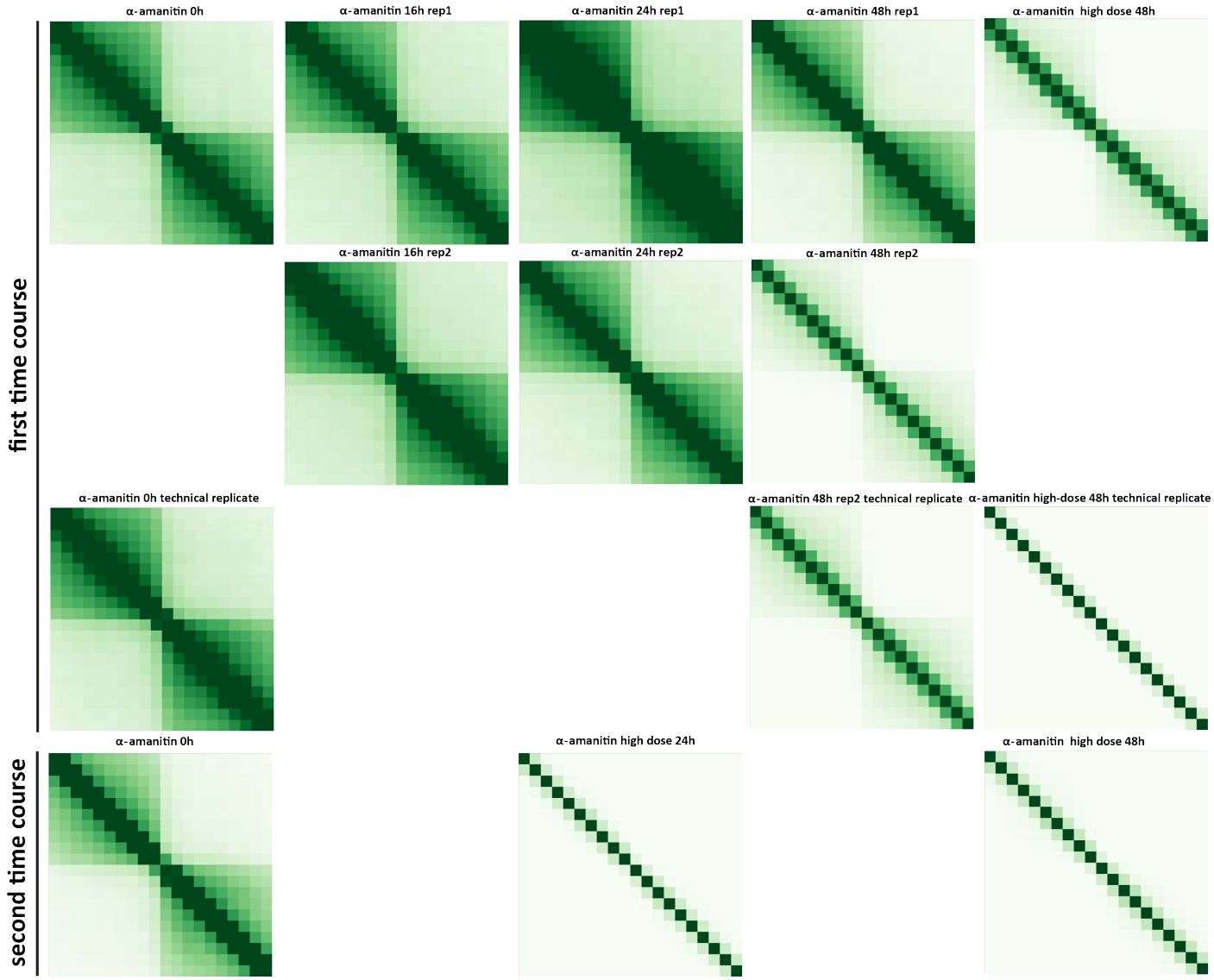

Supplementary Figure 24: Decompaction of dinoTADs upon transcriptional inhibition using α-amanitin. Shown are 50-kb resolution metaplots centered on dinoTAD domain boundaries. Two time courses were carried out following the outline presented in Figure 2B.

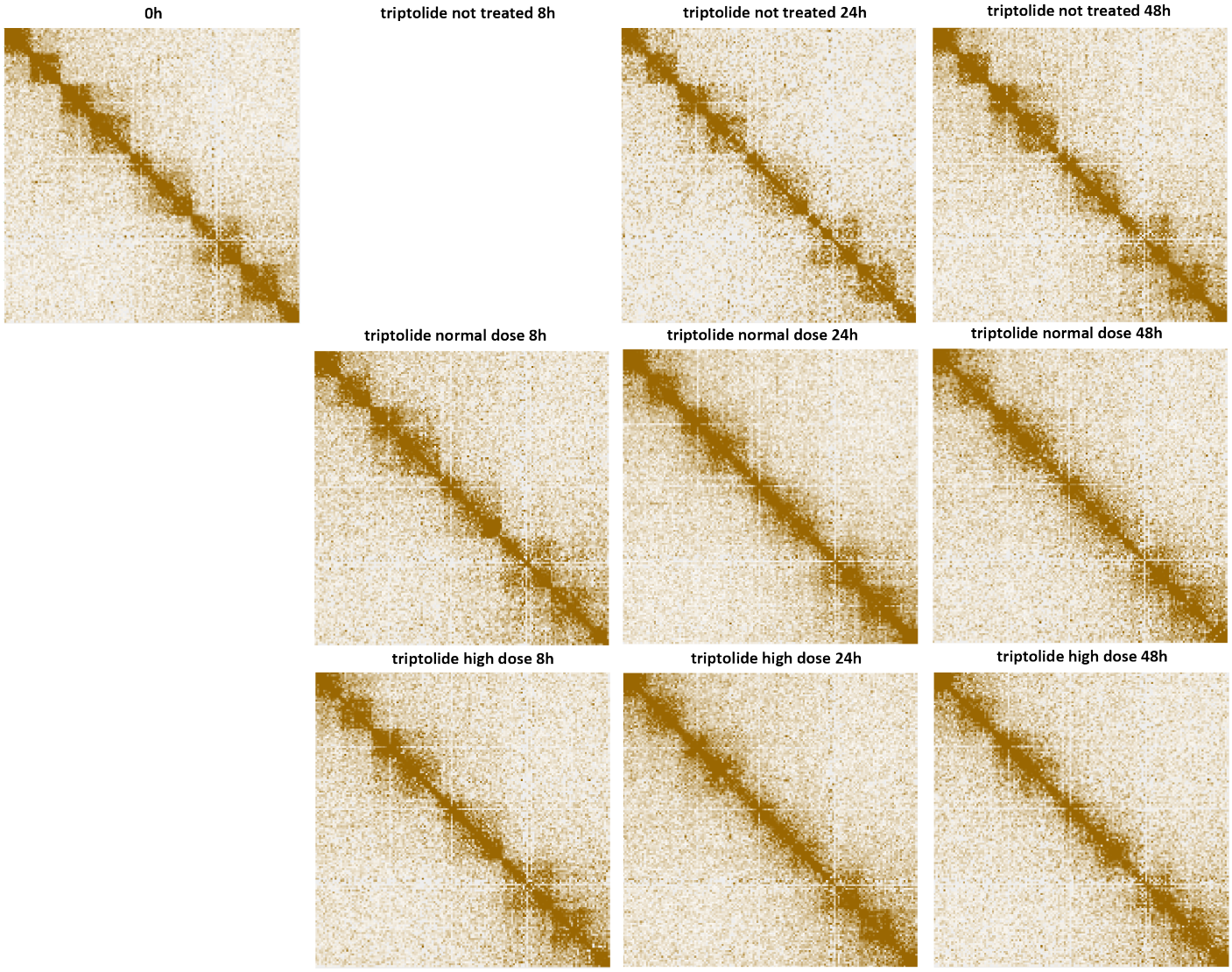

Supplementary Figure 25: Blurring of dinoTAD boundaries upon transcriptional inhibition using triptolide. Shown is pseudochromosome 10. The triptolide time course was carried out following the outline presented in Figure 2B.

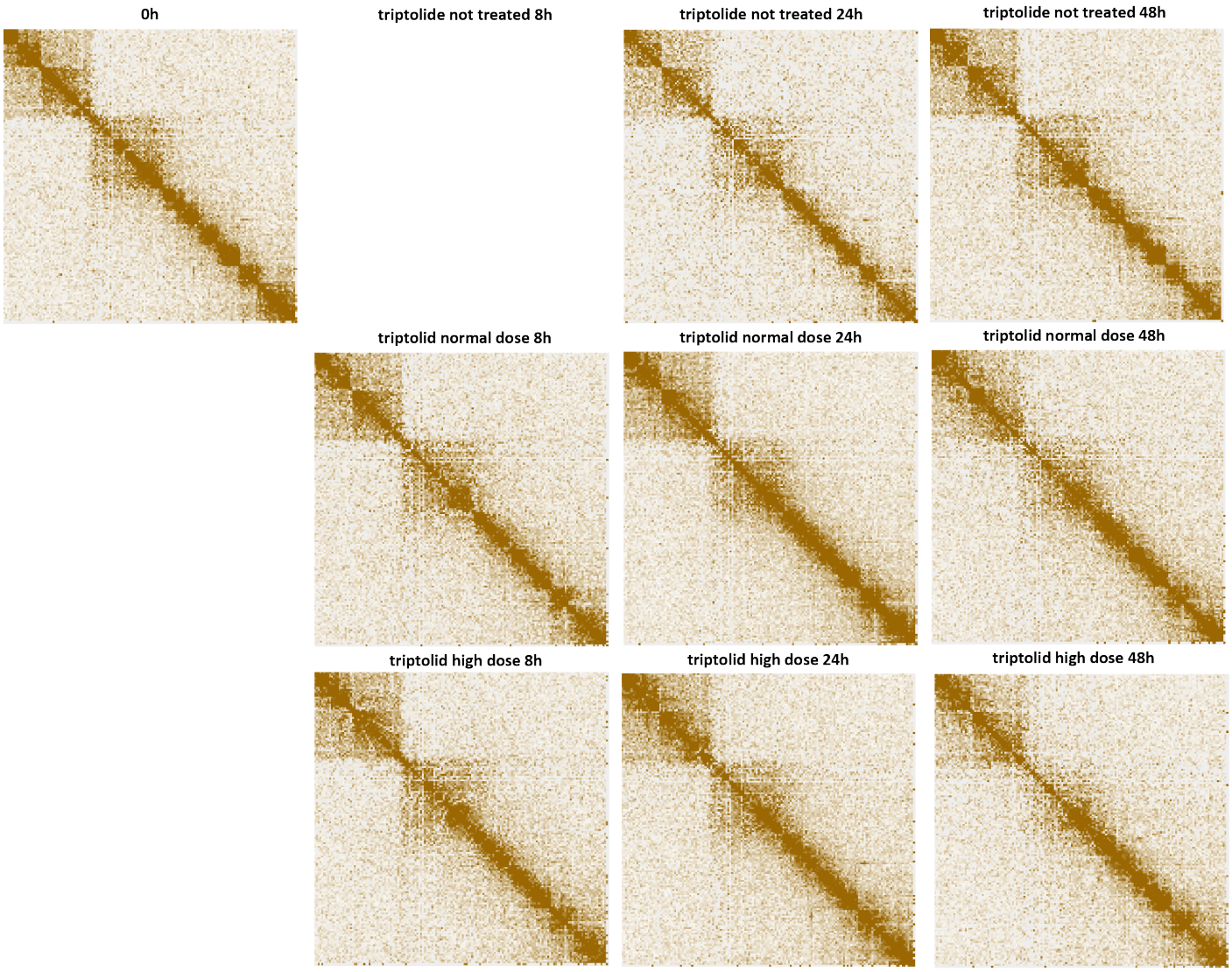

Supplementary Figure 26: Blurring of dinoTAD boundaries upon transcriptional inhibition using triptolide. Shown is pseudochromosome 17. The triptolide time course was carried out following the outline presented in Figure 2B.

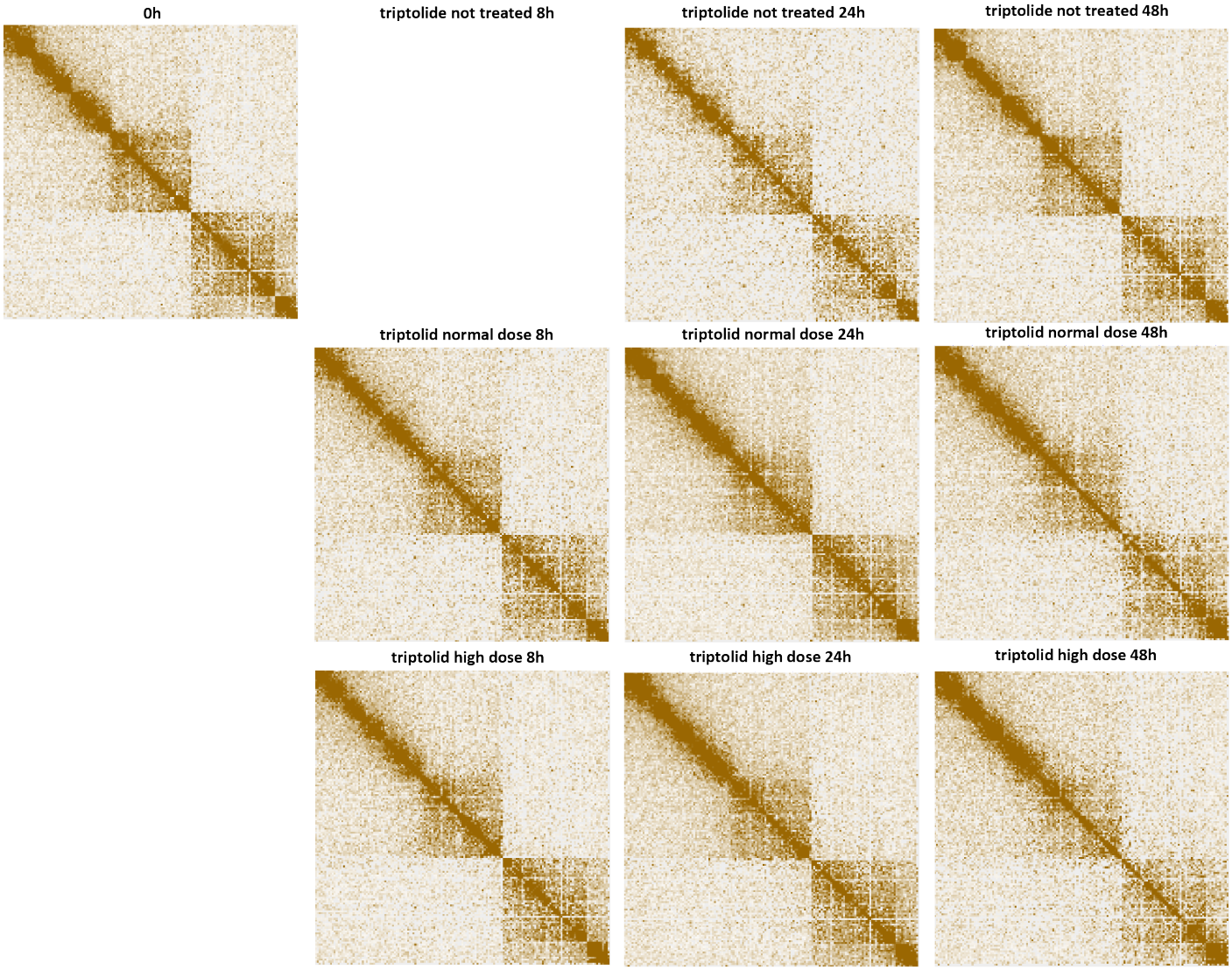

Supplementary Figure 27: Blurring of dinoTAD boundaries upon transcriptional inhibition using triptolide. Shown is pseudochromosome 18. The triptolide time course was carried out following the outline presented in Figure 2B.

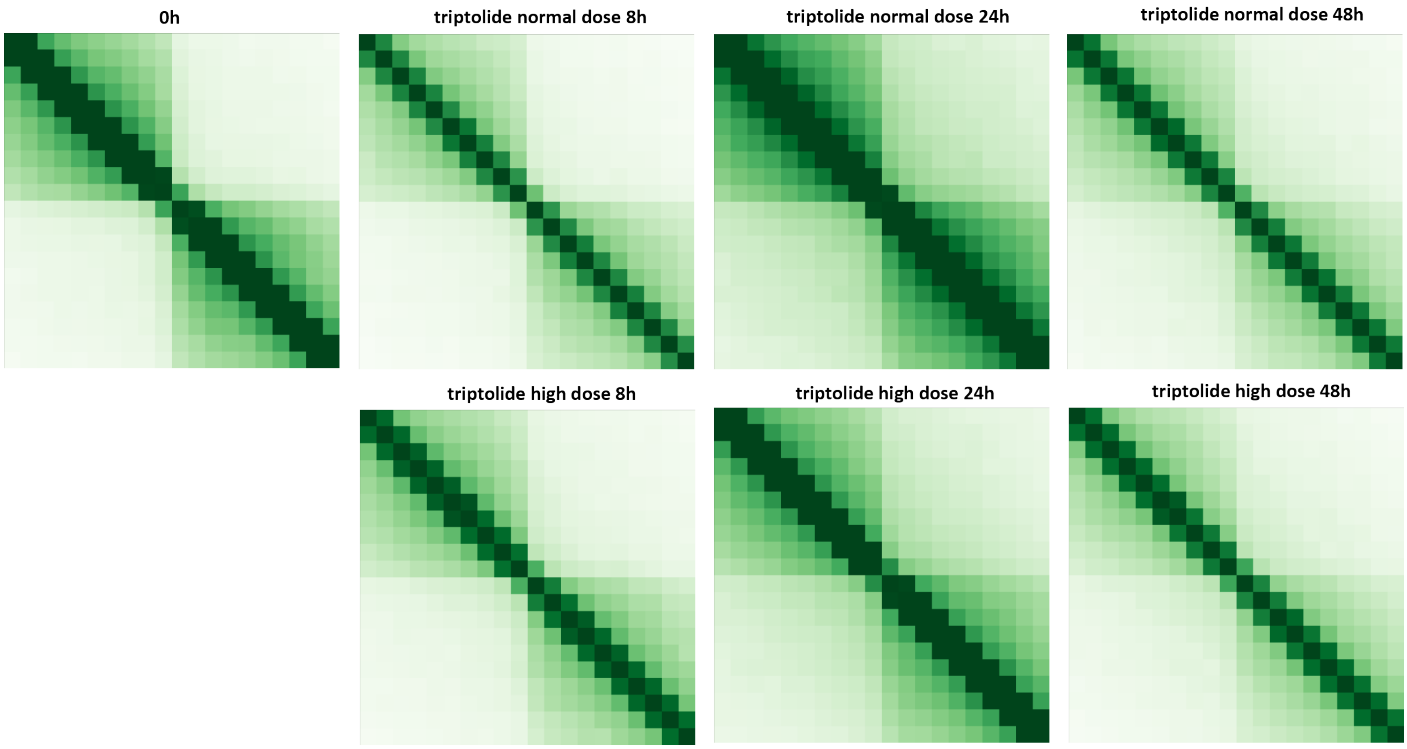

Supplementary Figure 28: Blurring of dinoTAD boundaries upon transcriptional inhibition using triptolide. Shown are 50-kb resolution metaplots centered on dinoTAD domain boundaries. The triptolide time course was carried out following the outline presented in Figure 2B.